Non-Newtonian ViRheometry via Similarity Analysis: Supplementary Material A

MITSUKI HAMAMICHI, Aoyama Gakuin University (AGU), Japan
KENTARO NAGASAWA, The University of Tokyo, Japan
MASATO OKADA, The University of Tokyo, Japan
RYOHEI SETO, Wenzhou Institute, University of Chinese Academy of Sciences / Oujiang Laboratory, China
YONGHAO YUE, Aoyama Gakuin University (AGU), Japan

CCS Concepts: • **Computing methodologies** → **Physical simulation**.

Additional Key Words and Phrases: Material parameter estimation, Herschel–Bulkley, shear thinning fluids, large-scale inclusions, video-based estimation

ACM Reference Format:
Mitsuki Hamamichi, Kentaro Nagasawa, Masato Okada, Ryohei Seto, and Yonghao Yue. 2023. Non-Newtonian ViRheometry via Similarity Analysis: Supplementary Material A. *ACM Trans. Graph.* 42, 6, Article 193SA (December 2023), 17 pages. https://doi.org/10.1145/3618310

1 DETAILED DISCRETE RETURN MAPPING

1.1 Scalar Return Mapping

We first show the discrete return mapping for solving the following flow rule appeared in Appendix B of our main paper:

$$\mathcal{L}_{\boldsymbol{v}}\mathbf{b}_{\mathrm{e}} = -\dot{\gamma}_{\mathrm{HB}}\frac{\sqrt{2}}{d}\operatorname{tr}[\mathbf{b}_{\mathrm{e}}]\frac{\operatorname{dev}[\boldsymbol{\sigma}]}{\|\operatorname{dev}[\boldsymbol{\sigma}]\|_{\mathrm{F}}}. \tag{1}$$

Directly discretizing (1) using backward Euler, we obtain

$$\mathbf{b}_{\mathrm{e},m+1} - \mathbf{b}_{\mathrm{e,pre}} = -\Delta t\dot{\gamma}_{\mathrm{HB},m+1}\frac{\sqrt{2}}{d}\operatorname{tr}[\mathbf{b}_{\mathrm{e},m+1}]\frac{\operatorname{dev}[\boldsymbol{\sigma}_{m+1}]}{\|\operatorname{dev}[\boldsymbol{\sigma}_{m+1}]\|_{\mathrm{F}}}. \tag{2}$$

Because the flow rule should be volume preserving, we have $\det[\mathbf{b}_{\mathrm{e},m+1}] = \det[\mathbf{b}_{\mathrm{e,pre}}]$. Dividing both sides by $(\det[\mathbf{b}_{\mathrm{e},m+1}])^{1/d}$ for normalization and plugging in $\boldsymbol{\sigma}_{m+1} = \frac{\mu}{J}\operatorname{dev}[\bar{\mathbf{b}}_{\mathrm{e},m+1}]$, where $J = (\det[\mathbf{b}_{\mathrm{e},m+1}])^{1/2}$, we have

$$\bar{\mathbf{b}}_{\mathrm{e},m+1} - \bar{\mathbf{b}}_{\mathrm{e,pre}} = -\Delta t\dot{\gamma}_{\mathrm{HB},m+1}\frac{\sqrt{2}}{d}\operatorname{tr}[\bar{\mathbf{b}}_{\mathrm{e},m+1}]\frac{\operatorname{dev}[\bar{\mathbf{b}}_{\mathrm{e},m+1}]}{\|\operatorname{dev}[\bar{\mathbf{b}}_{\mathrm{e},m+1}]\|_{\mathrm{F}}}. \tag{3}$$

Taking the trace of both sides, we have

$$\operatorname{tr}[\bar{\mathbf{b}}_{\mathrm{e},m+1}] - \operatorname{tr}[\bar{\mathbf{b}}_{\mathrm{e,pre}}] = 0. \tag{4}$$

Taking the deviator and multiply $\frac{\mu}{J}$ for both sides, and noting that $\boldsymbol{\sigma}_{m+1} = \frac{\mu}{J}\operatorname{dev}[\bar{\mathbf{b}}_{\mathrm{e},m+1}]$, we have

$$\boldsymbol{\sigma}_{\mathrm{s},m+1} - \boldsymbol{\sigma}_{\mathrm{s,pre}} = -\Delta t\frac{\mu}{J}\dot{\gamma}_{\mathrm{HB},m+1}\frac{\sqrt{2}}{d}\operatorname{tr}[\bar{\mathbf{b}}_{\mathrm{e,pre}}]\frac{\boldsymbol{\sigma}_{\mathrm{s},m+1}}{\|\boldsymbol{\sigma}_{\mathrm{s},m+1}\|_{\mathrm{F}}}. \tag{5}$$

Writing

$$\hat{\boldsymbol{\sigma}}_{\mathrm{s},m+1} = \frac{\boldsymbol{\sigma}_{\mathrm{s},m+1}}{\|\boldsymbol{\sigma}_{\mathrm{s},m+1}\|_{\mathrm{F}}},\ \text{and}\ \hat{\boldsymbol{\sigma}}_{\mathrm{s,pre}} = \frac{\boldsymbol{\sigma}_{\mathrm{s,pre}}}{\|\boldsymbol{\sigma}_{\mathrm{s,pre}}\|_{\mathrm{F}}} \tag{6}$$

for the 'directions' of the shear stress and decomposing the shear stress as

$$\boldsymbol{\sigma}_{\mathrm{s},m+1} = \sigma_{\mathrm{s},m+1}\hat{\boldsymbol{\sigma}}_{\mathrm{s},m+1},\ \text{and}\ \boldsymbol{\sigma}_{\mathrm{s,pre}} = \sigma_{\mathrm{s,pre}}\hat{\boldsymbol{\sigma}}_{\mathrm{s,pre}}, \tag{7}$$

we arrive at

$$\sigma_{\mathrm{s},m+1}\hat{\boldsymbol{\sigma}}_{\mathrm{s},m+1} - \sigma_{\mathrm{s,pre}}\hat{\boldsymbol{\sigma}}_{\mathrm{s,pre}} = -\Delta t\frac{\mu}{J}\dot{\gamma}_{\mathrm{HB},m+1}\frac{\sqrt{2}}{d}\operatorname{tr}[\bar{\mathbf{b}}_{\mathrm{e},m+1}]\hat{\boldsymbol{\sigma}}_{\mathrm{s},m+1}, \tag{8}$$

from which we notice the directions have not changed:

$$\hat{\boldsymbol{\sigma}}_{\mathrm{s},m+1} = \hat{\boldsymbol{\sigma}}_{\mathrm{s,pre}}. \tag{9}$$

Hence it suffices to solve the scalar part only:

$$\sigma_{\mathrm{s},m+1} - \sigma_{\mathrm{s,pre}} = -\frac{\sqrt{2}}{d}\Delta t\frac{\mu}{J}\operatorname{tr}[\bar{\mathbf{b}}_{\mathrm{e,pre}}]\left(\frac{\frac{1}{\sqrt{2}}\sigma_{\mathrm{s},m+1} - \sigma_{\mathrm{Y}}}{\eta}\right)^{1/n}, \tag{10}$$

which we solve via Newton method. After finding $\sigma_{\mathrm{s},m+1}$, we have

$$\bar{\mathbf{b}}_{\mathrm{e},m+1} = \frac{1}{d}\operatorname{tr}[\bar{\mathbf{b}}_{\mathrm{e,pre}}]\mathbf{I} + \frac{J}{\mu}\sigma_{\mathrm{s},m+1}\hat{\boldsymbol{\sigma}}_{\mathrm{s,pre}}. \tag{11}$$

We then normalize $\bar{\mathbf{b}}_{\mathrm{e},m+1}$ to have a unit determinant and compute $\mathbf{b}_{\mathrm{e},m+1}$ as

$$\mathbf{b}_{\mathrm{e},m+1} = \left(\frac{\det[\mathbf{b}_{\mathrm{e,pre}}]}{\det[\bar{\mathbf{b}}_{\mathrm{e},m+1}]}\right)^{1/d}\bar{\mathbf{b}}_{\mathrm{e},m+1}. \tag{12}$$

1.2 Solving in the Eigenspace

Next, we discuss solving

$$\mathbf{b}_{\mathrm{e},m+1} - \mathbf{b}_{\mathrm{e,pre}} = -\Delta t\dot{\gamma}_{\mathrm{HB},m+1}\left(\sqrt{2}\frac{\operatorname{dev}[\boldsymbol{\sigma}_{m+1}]}{\|\operatorname{dev}[\boldsymbol{\sigma}_{m+1}]\|_{\mathrm{F}}}\right)\mathbf{b}_{\mathrm{e},m+1} \tag{13}$$

without making the approximation.

Rearranging the terms, we have

$$\mathbf{b}_{\mathrm{e,pre}} = \mathbf{b}_{\mathrm{e},m+1} + \Delta t\dot{\gamma}_{\mathrm{HB},m+1}\left(\sqrt{2}\frac{\operatorname{dev}[\mathbf{b}_{\mathrm{e},m+1}]}{\|\operatorname{dev}[\mathbf{b}_{\mathrm{e},m+1}]\|_{\mathrm{F}}}\right)\mathbf{b}_{\mathrm{e},m+1}. \tag{14}$$

Let the eigendecomposition of $\mathbf{b}_{\mathrm{e},m+1}$ be given by

$$\mathbf{b}_{\mathrm{e},m+1} = \mathbf{Q}_{m+1}\boldsymbol{\Lambda}_{m+1}\mathbf{Q}_{m+1}^{\top}. \tag{15}$$

Authors' addresses: Mitsuki Hamamichi, Aoyama Gakuin University (AGU), Japan; Kentaro Nagasawa, The University of Tokyo, Japan; Masato Okada, The University of Tokyo, Kiban 701, Kashiwa-no-ha 5-1-5, Kashiwa-shi, Chiba, 277-8561, Japan; Ryohei Seto, Wenzhou Institute, University of Chinese Academy of Sciences / Oujiang Laboratory, Wenzhou, Zhejiang, 325000, China; Yonghao Yue, Aoyama Gakuin University (AGU), O-525, Fuchinobe 5-10-1, Chuo-ku, Sagamihara, Kanagawa, 252-5258, Japan, yonghao@it.aoyama.ac.jp.

0730-0301/2023/12-ART193SA
https://doi.org/10.1145/3618310

We have

$$\begin{aligned}\operatorname{dev}[\mathbf{b}_{\mathrm{e},m+1}] &= \mathbf{Q}_{m+1}\boldsymbol{\Lambda}_{m+1}\mathbf{Q}_{m+1}^{\top} - \frac{1}{d}\operatorname{tr}[\mathbf{Q}_{m+1}\boldsymbol{\Lambda}_{m+1}\mathbf{Q}_{m+1}^{\top}]\mathbf{I} \\ &= \mathbf{Q}_{m+1}\left(\boldsymbol{\Lambda}_{m+1} - \frac{1}{d}\operatorname{tr}[\boldsymbol{\Lambda}_{m+1}]\mathbf{I}\right)\mathbf{Q}_{m+1}^{\top} = \mathbf{Q}_{m+1}\operatorname{dev}[\boldsymbol{\Lambda}_{m+1}]\mathbf{Q}_{m+1}^{\top}.\end{aligned} \tag{16}$$

Thus, we have

$$\mathbf{b}_{\mathrm{e,pre}} = \mathbf{Q}_{m+1}\left(\boldsymbol{\Lambda}_{m+1} + \sqrt{2}\Delta t\dot{\gamma}_{\mathrm{HB},m+1}\left(\frac{\operatorname{dev}[\boldsymbol{\Lambda}_{m+1}]\boldsymbol{\Lambda}_{m+1}}{\|\operatorname{dev}[\boldsymbol{\Lambda}_{m+1}]\|_{\mathrm{F}}}\right)\right)\mathbf{Q}_{m+1}^{\top}. \tag{17}$$

Note that the part sandwiched by $\mathbf{Q}_{m+1}$ and $\mathbf{Q}_{m+1}^{\top}$ is diagonal, hence this gives the eigendecomposition of $\mathbf{b}_{\mathrm{e,pre}}$, so we know that the eigenvectors remain unchanged. Letting the eigenvalues of $\mathbf{b}_{\mathrm{e,pre}}$ be $\boldsymbol{\Lambda}_{\mathrm{pre}}$, we arrive at a system in the (diagonal) eigenspace as

$$\boldsymbol{\Lambda}_{\mathrm{pre}} = \boldsymbol{\Lambda}_{m+1} + \sqrt{2}\Delta t\dot{\gamma}_{\mathrm{HB},m+1}\left(\frac{\operatorname{dev}[\boldsymbol{\Lambda}_{m+1}]\boldsymbol{\Lambda}_{m+1}}{\|\operatorname{dev}[\boldsymbol{\Lambda}_{m+1}]\|_{\mathrm{F}}}\right), \tag{18}$$

which can be solved via Newton method. For the simple shear example discussed in the main paper, this would result in almost identical solutions as those from Section 1.1.

1.3 Analytical Form

We could also follow the procedure by Fei et al. [2019] to 'postpone' the discretization by first turning (1) into a scalar differential equation. Dividing both sides of (1) by $(\det[\mathbf{b}_{\mathrm{e},m+1}])^{1/d}$, we have

$$\frac{d\bar{\mathbf{b}}_{\mathrm{e}}}{dt} = -\frac{\sqrt{2}}{d}\operatorname{tr}[\bar{\mathbf{b}}_{\mathrm{e}}]\dot{\gamma}_{\mathrm{HB}}\frac{\operatorname{dev}[\bar{\mathbf{b}}_{\mathrm{e}}]}{\|\operatorname{dev}[\bar{\mathbf{b}}_{\mathrm{e}}]\|_{\mathrm{F}}}. \tag{19}$$

Noting that

$$\frac{d\operatorname{tr}[\bar{\mathbf{b}}_{\mathrm{e}}]}{dt} = \frac{\partial\operatorname{tr}[\bar{\mathbf{b}}_{\mathrm{e}}]}{\partial\bar{\mathbf{b}}_{\mathrm{e}}} : \frac{d\bar{\mathbf{b}}_{\mathrm{e}}}{dt} = \mathbf{I} : \frac{d\bar{\mathbf{b}}_{\mathrm{e}}}{dt} = \operatorname{tr}[\frac{d\bar{\mathbf{b}}_{\mathrm{e}}}{dt}] = 0, \tag{20}$$

taking the deviator of (19) and multiplying $\frac{\mu}{J}$ to both sides, we have

$$\frac{d\frac{\mu}{J}\operatorname{dev}[\bar{\mathbf{b}}_{\mathrm{e}}]}{dt} = -\frac{\sqrt{2}}{d}\frac{\mu}{J}\operatorname{tr}[\bar{\mathbf{b}}_{\mathrm{e}}]\dot{\gamma}_{\mathrm{HB}}\frac{\frac{\mu}{J}\operatorname{dev}[\bar{\mathbf{b}}_{\mathrm{e}}]}{\|\frac{\mu}{J}\operatorname{dev}[\bar{\mathbf{b}}_{\mathrm{e}}]\|_{\mathrm{F}}}, \tag{21}$$

which gives

$$\frac{d\boldsymbol{\sigma}_{\mathrm{s}}}{dt} = -\frac{\sqrt{2}}{d}\frac{\mu}{J}\operatorname{tr}[\bar{\mathbf{b}}_{\mathrm{e}}]\left(\frac{\max\left(0, \frac{1}{\sqrt{2}}\sigma_{\mathrm{s}} - \sigma_{\mathrm{Y}}\right)}{\eta}\right)^{1/n}\hat{\boldsymbol{\sigma}}_{\mathrm{s}}\boldsymbol{\sigma}_{\mathrm{s}}. \tag{22}$$

Extracting its scalar part, we have

$$\frac{d\sigma_{\mathrm{s}}}{dt} = -\frac{\sqrt{2}}{d}\frac{\mu}{J}\operatorname{tr}[\bar{\mathbf{b}}_{\mathrm{e}}]\left(\frac{\max\left(0, \frac{1}{\sqrt{2}}\sigma_{\mathrm{s}} - \sigma_{\mathrm{Y}}\right)}{\eta}\right)^{1/n}, \tag{23}$$

which admits an analytic solution given by

$$\begin{aligned}\sigma_{\mathrm{s},m+1} = \sqrt{2}\sigma_{\mathrm{Y}} + \Bigg[&\left(\sigma_{\mathrm{s,pre}} - \sqrt{2}\sigma_{\mathrm{Y}}\right)^{\frac{n-1}{n}} \\ &- \left(1 - \frac{1}{n}\right)\frac{\sqrt{2}}{d}\mu\operatorname{tr}[\bar{\mathbf{b}}_{\mathrm{e,pre}}]\left(\frac{1}{\sqrt{2}\eta}\right)^{1/n}\Delta t\Bigg]^{\frac{n}{n-1}}.\end{aligned} \tag{24}$$

Then, the rest of the procedure follows (11). This approach is good enough in practice, and is the most efficient among the three approaches discussed in this Section. However, we note that this approach introduces an error in terms of the terminal stress of the order $\Delta\sigma_{\mathrm{s}} \approx -\frac{1}{2}\mu\Delta t\dot{\gamma}$. For safety, we use the approach in Section 1.1 in our method.

Here we derive the error in terminal stress. For simplicity, we consider the 1D case, where the evolution of the shear stress is given by

$$\dot{\sigma}_{\mathrm{s}} = \mu\dot{\varepsilon} - \frac{\mu}{\eta^{1/n}}(\sigma_{\mathrm{s}} - \sigma_{\mathrm{Y}})^{1/n}. \tag{25}$$

Note that we are writing $\dot{\varepsilon}$ in place of $\dot{\gamma}$. The corresponding elastic prediction is

$$\sigma_{\mathrm{s,pre}} = \sigma_{\mathrm{s}} + \Delta t\mu\dot{\varepsilon}. \tag{26}$$

Defining

$$\sigma_{\mathrm{ex}} := \sigma_{\mathrm{s}} - \sigma_{\mathrm{Y}}, \tag{27}$$

for the corresponding analytic form of the plastic correction, we then have

$$\dot{\sigma}_{\mathrm{ex}} = -\frac{\mu}{\eta^{1/n}}{\sigma_{\mathrm{ex}}}^{1/n}. \tag{28}$$

For both sides, dividing by ${\sigma_{\mathrm{ex}}}^{1/n}$, multiplying by dt, and integrating, we have

$$\int_{t_{\mathrm{pre}}}^{t_{m+1}} {\sigma_{\mathrm{ex}}}^{-1/n} d\sigma_{\mathrm{ex}} = -\int_{t_{\mathrm{pre}}}^{t_{m+1}} \mu\eta^{-1/n} dt, \tag{29}$$

which gives

$$\sigma_{\mathrm{ex},m+1} = \left[{\sigma_{\mathrm{ex,pre}}}^{1-1/n} - \frac{n-1}{n}\mu\eta^{-1/n}\Delta t\right]^{\frac{n}{n-1}}. \tag{30}$$

Hence,

$$\sigma_{\mathrm{s},m+1} = \sigma_{\mathrm{Y}} + \left[(\sigma_{\mathrm{s,pre}} - \sigma_{\mathrm{Y}})^{1-1/n} - \frac{n-1}{n}\mu\eta^{-1/n}\Delta t\right]^{\frac{n}{n-1}}. \tag{31}$$

At t_∞, we have $\sigma_{\mathrm{s},m} = \sigma_{\mathrm{s},m+1} = \sigma_{\mathrm{s},\infty}$, hence,

$$\frac{n}{n-1}(\sigma_{\mathrm{s},\infty} - \sigma_{\mathrm{Y}})^{1-1/n} - \frac{n}{n-1}(\sigma_{\mathrm{s},\infty} + \Delta t\mu\dot{\varepsilon} - \sigma_{\mathrm{Y}})^{1-1/n} = -\mu\eta^{-1/n}\Delta t \tag{32}$$

Now, we substitute $\tilde{\sigma}_{\mathrm{s},\infty} = \sigma_{\mathrm{Y}} + \eta\dot{\varepsilon}^n$ and $\sigma_{\mathrm{s},\infty} = \tilde{\sigma}_{\mathrm{s},\infty} + \Delta\sigma_{\mathrm{s}}$, and evaluate $\Delta\sigma_{\mathrm{s}}$. Then, (32) becomes

$$(\eta\dot{\varepsilon}^n + \Delta\sigma_{\mathrm{s}})^{1-1/n} - (\eta\dot{\varepsilon}^n + \Delta\sigma_{\mathrm{s}} + \Delta t\mu\dot{\varepsilon})^{1-1/n} = -\frac{n-1}{n}\mu\eta^{-1/n}\Delta t. \tag{33}$$

Set $f(x) := x^{1-1/n}$, and expand up to second order, we have

$$\begin{aligned}f(x+\Delta x) &= f(x) + \Delta x f'(x) + \frac{1}{2}(\Delta x)^2 f''(x) + O((\Delta x)^3) \\ &= x^{1-1/n} + \Delta x\left(1 - \frac{1}{n}\right)x^{-1/n} - \frac{1}{2}(\Delta x)^2\frac{1}{n}\left(1 - \frac{1}{n}\right)x^{-1/n-1} + O((\Delta x)^3).\end{aligned} \tag{34}$$

Using the above expansion for $x = \eta\dot{\varepsilon}^n + \Delta\sigma_{\mathrm{s}}$ and $\Delta x = \Delta t\mu\dot{\varepsilon}$, and substituting into (33) then rearrange, we obtain

$$\Delta\sigma_{\mathrm{s}} \approx -\frac{1}{2}\mu\dot{\varepsilon}\Delta t. \tag{35}$$

2 DERIVATION FOR PLANE POISEUILLE FLOW

We start from the equation of motion

$$\rho \frac{D\boldsymbol{v}}{Dt} = -\nabla p + \nabla \cdot \boldsymbol{\sigma}_{\mathrm{s}}, \tag{36}$$

where ρ is the material density, $\frac{D\cdot}{Dt}$ is the material derivative, and p is the pressure. The constant pressure gradient assumption gives rise to $-\nabla p = (P, 0)$. The steady flow assumes the flow is solely in the x direction, with its x component v_x depending only on y: $\boldsymbol{v} = (v_x(y), 0)$. In addition, $\boldsymbol{v}$ does not depend on time and hence $\frac{\partial \boldsymbol{v}}{\partial t} = 0$. Hence $(\boldsymbol{v} \cdot \nabla)\boldsymbol{v} = \mathbf{0}$. Combined together, we have $\frac{D\boldsymbol{v}}{Dt} = \mathbf{0}$. Like the case of simple shear, the diagonal components of $\mathbf{D} = \mathbf{L} + \mathbf{L}^\top$ vanish. Following (14) in the main paper, we have

$$\dot{\gamma} = \sqrt{\frac{\mathbf{D} : \mathbf{D}}{2}} = \left|\frac{\partial v_x}{\partial y}\right|, \text{ and } \sigma_{\mathrm{s}} = \sqrt{\frac{\boldsymbol{\sigma}_{\mathrm{s}} : \boldsymbol{\sigma}_{\mathrm{s}}}{2}} = \left|\sigma_{xy}\right|, \tag{37}$$

where σ_{xy} is the off-diagonal component of $\boldsymbol{\sigma}_{\mathrm{s}}$. When the yield condition is violated (i.e., $\left|\sigma_{xy}\right| \geq \sigma_{\mathrm{Y}}$), the fluid flows, and the Herschel–Bulkley model relates the flow rate and shear stress via

$$\boldsymbol{\sigma}_{\mathrm{s}} = \left(\sigma_{\mathrm{Y}} + \eta \dot{\gamma}^n\right) \frac{\mathbf{D}}{\dot{\gamma}}, \text{ and } \sigma_{xy} = \left(\sigma_{\mathrm{Y}} + \eta \dot{\gamma}^n\right) \operatorname{sgn}\left(\frac{\partial v_x}{\partial y}\right), \tag{38}$$

hence the diagonal components of $\boldsymbol{\sigma}_{\mathrm{s}}$ vanish as well. When the yield condition is not violated ($\sigma_{xy} < \sigma_{\mathrm{Y}}$), the flow stags, leading to the plug region with $\dot{\gamma} = 0$.

The equation of motion now reduces to

$$\begin{cases} P + \frac{\partial \sigma_{xy}}{\partial y} = 0, & \text{for the } x \text{ component,} \\ \frac{\partial \sigma_{xy}}{\partial x} = 0, & \text{for the } y \text{ component,} \end{cases} \tag{39}$$

hence σ_{xy} is a function of y only.

For the boundary condition, we have $\frac{\partial v_x(y)}{\partial y} = 0$ at $y = \pm l$ where l is the yield surface between the flowing and plug regions, and $v_x(y) = 0$ at $y = \pm L$ due to the non-slip condition. Integrating (39) along y, and applying the yield condition $\sigma_{xy} = \mp\sigma_{\mathrm{Y}}$ at $y = \pm l$, we obtain

$$\sigma_{xy} = -Py, \text{ and } l = \frac{\sigma_{\mathrm{Y}}}{P}. \tag{40}$$

Substituting into (38) and integrating along y, we have for the plug region ($|y| \leq l$) a spatially constant velocity (we are adding $\mathbf{M}$ and S^{PP} as the subscripts to clarify the dependency),

$$v_{x,\mathbf{M};\mathrm{S}^{\mathrm{PP}}}(y) = v^{(\mathrm{Max})}_{x,\mathbf{M};\mathrm{S}^{\mathrm{PP}}} := \frac{n}{n+1}\left(\frac{P}{\eta}\right)^{1/n} (L-l)^{\frac{n+1}{n}}, \tag{41}$$

and for the flowing region ($l < |y| < L$),

$$v_{x,\mathbf{M};\mathrm{S}^{\mathrm{PP}}}(y) = v^{(\mathrm{Max})}_{x,\mathbf{M};\mathrm{S}^{\mathrm{PP}}} \zeta_{\mathbf{M};\mathrm{S}^{\mathrm{PP}}}(y), \tag{42}$$

where

$$\zeta_{\mathbf{M};\mathrm{S}^{\mathrm{PP}}}(y) := 1 - \left(\frac{|y| - l}{L - l}\right)^{\frac{n+1}{n}} \tag{43}$$

is the decay ratio satisfying $0 \leq \zeta_{\mathbf{M};\mathrm{S}^{\mathrm{PP}}}(y) \leq 1$ for $l \leq |y| \leq L$.

3 ANALYTIC PLANE POISEUILLE HESSIAN

Starting from

$$\mathbf{H}^{\mathrm{PP}}_{\mathbf{M};\mathrm{S}^{\mathrm{PP}}} = 2\int_0^L \boldsymbol{G}_{\mathbf{M};\mathrm{S}^{\mathrm{PP}}}(y)^\top \boldsymbol{G}_{\mathbf{M};\mathrm{S}^{\mathrm{PP}}}(y) dy, \tag{44}$$

we split the integral into the part from 0 to l and the part from l to L.

For $0 \leq y \leq l$, we had $v_{x,\mathbf{M};\mathrm{S}^{\mathrm{PP}}}(y) = v^{(\mathrm{Max})}_{x,\mathbf{M};\mathrm{S}^{\mathrm{PP}}}$. We write its derivative $\frac{\partial v^{(\mathrm{Max})}_{x,\mathbf{M};\mathrm{S}^{\mathrm{PP}}}}{\partial \mathbf{M}}$ as

$$\frac{\partial v^{(\mathrm{Max})}_{x,\mathbf{M};\mathrm{S}^{\mathrm{PP}}}}{\partial \mathbf{M}} = U_1(\eta, n, \sigma_{\mathrm{Y}}) U_2(\eta, n, \sigma_{\mathrm{Y}}) U_3(\eta, n, \sigma_{\mathrm{Y}}), \tag{45}$$

where $U_1(\eta, n, \sigma_{\mathrm{Y}}) = \frac{n}{n+1}$, $U_2(\eta, n, \sigma_{\mathrm{Y}}) = \left(\frac{P}{\eta}\right)^{1/n}$, and $U_3(\eta, n, \sigma_{\mathrm{Y}}) = \left(L - \frac{\sigma_{\mathrm{Y}}}{P}\right)^{\frac{n+1}{n}}$.

Using the derivatives summarized in Table 1, we have $\frac{\partial v^{(\mathrm{Max})}_{x,\mathbf{M};\mathrm{S}^{\mathrm{PP}}}}{\partial \eta} = LA_\eta$, $\frac{\partial v^{(\mathrm{Max})}_{x,\mathbf{M};\mathrm{S}^{\mathrm{PP}}}}{\partial n} = LA_n$, and $\frac{\partial v^{(\mathrm{Max})}_{x,\mathbf{M};\mathrm{S}^{\mathrm{PP}}}}{\partial \sigma_{\mathrm{Y}}} = LA_{\sigma_{\mathrm{Y}}}$, where

$$A_\eta := -\frac{1}{n+1}\frac{1}{PL}\left(\frac{PL - \sigma_{\mathrm{Y}}}{\eta}\right)^{\frac{n+1}{n}}, \tag{46}$$

$$A_n := \frac{\eta}{PL}\left(\frac{PL - \sigma_{\mathrm{Y}}}{\eta}\right)^{\frac{n+1}{n}} \left(\frac{1}{(n+1)^2} - \frac{1}{n(n+1)}\left(\log\frac{PL - \sigma_{\mathrm{Y}}}{\eta}\right)\right), \tag{47}$$

$$A_{\sigma_{\mathrm{Y}}} := -\frac{1}{PL}\left(\frac{PL - \sigma_{\mathrm{Y}}}{\eta}\right)^{\frac{1}{n}}. \tag{48}$$

For $0 \leq y \leq l$, we then have

$$2\int_0^l \boldsymbol{G}_{\mathbf{M};\mathrm{S}^{\mathrm{PP}}}(y) \boldsymbol{G}_{\mathbf{M};\mathrm{S}^{\mathrm{PP}}}(y)^\top dy = 2lL^2 \begin{pmatrix} A_\eta^2 & A_\eta A_n & A_\eta A_{\sigma_{\mathrm{Y}}} \\ A_\eta A_n & A_n^2 & A_n A_{\sigma_{\mathrm{Y}}} \\ A_\eta A_{\sigma_{\mathrm{Y}}} & A_n A_{\sigma_{\mathrm{Y}}} & A_{\sigma_{\mathrm{Y}}}^2 \end{pmatrix} \tag{49}$$

$$= 2L^3 \frac{\sigma_{\mathrm{Y}}}{PL} \begin{pmatrix} A_\eta^2 & A_\eta A_n & A_\eta A_{\sigma_{\mathrm{Y}}} \\ A_\eta A_n & A_n^2 & A_n A_{\sigma_{\mathrm{Y}}} \\ A_\eta A_{\sigma_{\mathrm{Y}}} & A_n A_{\sigma_{\mathrm{Y}}} & A_{\sigma_{\mathrm{Y}}}^2 \end{pmatrix}. \tag{50}$$

Next, for $l \leq y \leq L$, we use short hand notations $v_{x\eta}(y)$, $v_{xn}(y)$, and $v_{x\sigma_{\mathrm{Y}}}(y)$ to indicate $\frac{\partial v_{x,\mathbf{M};\mathrm{S}^{\mathrm{PP}}}(y)}{\partial \eta}$, $\frac{\partial v_{x,\mathbf{M};\mathrm{S}^{\mathrm{PP}}}(y)}{\partial n}$, and $\frac{\partial v_{x,\mathbf{M};\mathrm{S}^{\mathrm{PP}}}(y)}{\partial \sigma_{\mathrm{Y}}}$, respectively, and using the derivatives summarized in Table 2 in addition to Table 1, we have

$$v_{x\eta}(y) = LA_\eta - LA_\eta\left(\frac{y-l}{L-l}\right)^{\frac{n+1}{n}}, \tag{51}$$

$$v_{xn}(y) = LA_n - LA_n\left(\frac{y-l}{L-l}\right)^{\frac{n+1}{n}} + LB_n\left(\frac{y-l}{L-l}\right)^{\frac{n+1}{n}} \log\left(\frac{y-l}{L-l}\right), \tag{52}$$

$$v_{x\sigma_{\mathrm{Y}}}(y) = LA_{\sigma_{\mathrm{Y}}} - LA_{\sigma_{\mathrm{Y}}}\left(\frac{y-l}{L-l}\right)^{\frac{1}{n}}, \tag{53}$$

where

$$B_n := \frac{1}{n(n+1)}\left(\frac{PL - \sigma_{\mathrm{Y}}}{\eta}\right)^{\frac{1}{n}} \left(1 - \frac{\sigma_{\mathrm{Y}}}{PL}\right). \tag{54}$$

Then,

$$\begin{aligned}&\boldsymbol{G}_{\mathbf{M};\mathbf{S}^{\mathrm{PP}}}(y)^{\top}\boldsymbol{G}_{\mathbf{M};\mathbf{S}^{\mathrm{PP}}}(y)\\&=\begin{pmatrix}\left(v_{x\eta}(y)\right)^2 & v_{x\eta}(y)v_{xn}(y) & v_{x\eta}(y)v_{x\sigma_{\mathrm{Y}}}(y)\\ v_{xn}(y)v_{x\eta}(y) & \left(v_{xn}(y)\right)^2 & v_{xn}(y)v_{x\sigma_{\mathrm{Y}}}(y)\\ v_{x\sigma_{\mathrm{Y}}}(y)v_{x\eta}(y) & v_{x\sigma_{\mathrm{Y}}}(y)v_{xn}(y) & \left(v_{x\sigma_{\mathrm{Y}}}(y)\right)^2\end{pmatrix}.\end{aligned}\tag{55}$$

Using the following notations,

$$I_1(a,b,k) \coloneqq \int_a^b \left(\frac{y-l}{L-l}\right)^k dy, \tag{56}$$

$$I_2(a,b,k) \coloneqq \int_a^b \left(\frac{y-l}{L-l}\right)^k \log\left(\frac{y-l}{L-l}\right) dy, \tag{57}$$

$$I_3(a,b,k) \coloneqq \int_a^b \left(\frac{y-l}{L-l}\right)^k \left(\log\left(\frac{y-l}{L-l}\right)\right)^2 dy, \tag{58}$$

we have

$$\frac{1}{L^2}\int_l^L \left(v_{x\eta}(y)\right)^2 dy = A_\eta^2 I_1\left(l,L,\frac{2n+2}{n}\right) - 2A_\eta^2 I_1\left(l,L,\frac{n+1}{n}\right) + A_\eta^2(L-l), \tag{59}$$

$$\begin{aligned}&\frac{1}{L^2}\int_l^L v_{x\eta}(y)v_{xn}(y)dy = -2A_\eta A_n I_1\left(l,L,\frac{n+1}{n}\right) + A_\eta A_n(L-l)\\&+A_\eta A_n I_1\left(l,L,\frac{2n+2}{n}\right) - A_\eta B_n I_2\left(l,L,\frac{2n+2}{n}\right) + A_\eta B_n I_2\left(l,L,\frac{n+1}{n}\right),\end{aligned}\tag{60}$$

$$\begin{aligned}&\frac{1}{L^2}\int_l^L v_{x\eta}(y)v_{x\sigma_{\mathrm{Y}}}(y)dy = A_\eta A_{\sigma_{\mathrm{Y}}} I_1\left(l,L,\frac{2n+2}{n}\right) - A_\eta A_{\sigma_{\mathrm{Y}}} I_1\left(l,L,\frac{n+1}{n}\right)\\&- A_\eta A_{\sigma_{\mathrm{Y}}} I_1\left(l,L,\frac{1}{n}\right) + A_\eta A_{\sigma_{\mathrm{Y}}}(L-l),\end{aligned}\tag{61}$$

$$\begin{aligned}&\frac{1}{L^2}\int_l^L \left(v_{xn}(y)\right)^2 dy = B_n^2 I_3\left(l,L,\frac{2n+2}{n}\right) + A_n^2 I_1\left(l,L,\frac{2n+2}{n}\right) + A_n^2(L-l)\\&- 2A_nB_n I_2\left(l,L,\frac{n+1}{n}\right) - 2A_n^2 I_1\left(l,L,\frac{n+1}{n}\right),\end{aligned}\tag{62}$$

$$\begin{aligned}&\frac{1}{L^2}\int_l^L v_{xn}(y)v_{x\sigma_{\mathrm{Y}}}(y)dy = -A_nA_{\sigma_{\mathrm{Y}}} I_1\left(l,L,\frac{1}{n}\right) + A_nA_{\sigma_{\mathrm{Y}}}(L-l)\\&+A_nA_{\sigma_{\mathrm{Y}}} I_1\left(l,L,\frac{n+2}{n}\right) - A_nA_{\sigma_{\mathrm{Y}}} I_1\left(l,L,\frac{n+1}{n}\right) - B_nA_{\sigma_{\mathrm{Y}}} I_2\left(l,L,\frac{n+2}{n}\right)\\&+B_nA_{\sigma_{\mathrm{Y}}} I_2\left(l,L,\frac{n+1}{n}\right),\end{aligned}\tag{63}$$

$$\frac{1}{L^2}\int_l^L \left(v_{x\sigma_{\mathrm{Y}}}(y)\right)^2 dy = A_{\sigma_{\mathrm{Y}}}^2 I_1\left(l,L,\frac{2}{n}\right) - 2A_{\sigma_{\mathrm{Y}}}^2 I_1\left(l,L,\frac{1}{n}\right) + A_{\sigma_{\mathrm{Y}}}^2(L-l). \tag{64}$$

Using the results in Section 4, and combined with (49), we arrive at

$$\mathbf{H}^{\mathrm{PP}}_{\mathbf{M};\mathbf{S}^{\mathrm{PP}}} = L^3\tilde{\mathbf{H}}^{\mathrm{PP}}_{\mathbf{M};\mathbf{S}^{\mathrm{PP}}} = L^3\begin{pmatrix}\tilde{H}_{\eta\eta} & \tilde{H}_{\eta n} & \tilde{H}_{\eta\sigma_{\mathrm{Y}}}\\ \tilde{H}_{\eta n} & \tilde{H}_{nn} & \tilde{H}_{n\sigma_{\mathrm{Y}}}\\ \tilde{H}_{\eta\sigma_{\mathrm{Y}}} & \tilde{H}_{n\sigma_{\mathrm{Y}}} & \tilde{H}_{\sigma_{\mathrm{Y}}\sigma_{\mathrm{Y}}}\end{pmatrix}, \tag{65}$$

Table 1. Differentials of elements of $v^{(\mathrm{Max})}_{\boldsymbol{x},\mathbf{M};\mathbf{S}^{\mathrm{PP}}}$.

	$\frac{\partial}{\partial\eta}$	$\frac{\partial}{\partial n}$	$\frac{\partial}{\partial\sigma_{\mathrm{Y}}}$
$U_1 = \frac{n}{n+1}$	0	$\frac{1}{(n+1)^2}$	0
$U_2 = \left(\frac{P}{\eta}\right)^{1/n}$	$-\frac{1}{n\eta}\left(\frac{P}{\eta}\right)^{1/n}$	$-\frac{1}{n^2}\left(\frac{P}{\eta}\right)^{1/n}\log\frac{P}{\eta}$	0
$U_3 = \left(L-\frac{\sigma_{\mathrm{Y}}}{P}\right)^{\frac{n+1}{n}}$	0	$-\frac{1}{n^2}\left(L-\frac{\sigma_{\mathrm{Y}}}{P}\right)^{\frac{n+1}{n}}\log\left(L-\frac{\sigma_{\mathrm{Y}}}{P}\right)$	$-\frac{n+1}{n}\frac{1}{P}\left(L-\frac{\sigma_{\mathrm{Y}}}{P}\right)^{\frac{1}{n}}$

Table 2. Differentials of $\zeta_{\mathbf{M};\mathbf{S}^{\mathrm{PP}}}(y)$.

	$\frac{\partial}{\partial\eta}$	$\frac{\partial}{\partial n}$	$\frac{\partial}{\partial\sigma_{\mathrm{Y}}}$
ζ	0	$\left(\frac{y-l}{L-l}\right)^{\frac{n+1}{n}}\frac{1}{n^2}\log\left(\frac{y-l}{L-l}\right)$	$\frac{n+1}{n}\frac{1}{P(L-l)}\left(\left(\frac{y-l}{L-l}\right)^{\frac{1}{n}} - \left(\frac{y-l}{L-l}\right)^{\frac{n+1}{n}}\right)$

where

$$\tilde{H}_{\eta\eta} = 2\frac{\sigma_{\mathrm{Y}}}{PL}A_\eta^2 + 4\left(1-\frac{\sigma_{\mathrm{Y}}}{PL}\right)A_\eta^2 C_1, \tag{66}$$

$$\tilde{H}_{\eta n} = 2\frac{\sigma_{\mathrm{Y}}}{PL}A_\eta A_n + 2\left(1-\frac{\sigma_{\mathrm{Y}}}{PL}\right)\left(2A_\eta A_n C_1 - A_\eta B_n C_2\right), \tag{67}$$

$$\tilde{H}_{\eta\sigma_{\mathrm{Y}}} = 2\frac{\sigma_{\mathrm{Y}}}{PL}A_\eta A_{\sigma_{\mathrm{Y}}} + 2\left(1-\frac{\sigma_{\mathrm{Y}}}{PL}\right)A_\eta A_{\sigma_{\mathrm{Y}}} C_3, \tag{68}$$

$$\tilde{H}_{nn} = 2\frac{\sigma_{\mathrm{Y}}}{PL}A_n^2 + 4\left(1-\frac{\sigma_{\mathrm{Y}}}{PL}\right)\left(B_n^2 C_4 - A_nB_nC_2 + A_n^2 C_1\right), \tag{69}$$

$$\tilde{H}_{n\sigma_{\mathrm{Y}}} = 2\frac{\sigma_{\mathrm{Y}}}{PL}A_n A_{\sigma_{\mathrm{Y}}} + 2\left(1-\frac{\sigma_{\mathrm{Y}}}{PL}\right)\left(A_nA_{\sigma_{\mathrm{Y}}} C_3 - B_nA_{\sigma_{\mathrm{Y}}} C_5\right), \tag{70}$$

$$\tilde{H}_{\sigma_{\mathrm{Y}}\sigma_{\mathrm{Y}}} = 2\frac{\sigma_{\mathrm{Y}}}{PL}A_{\sigma_{\mathrm{Y}}}^2 + 4\left(1-\frac{\sigma_{\mathrm{Y}}}{PL}\right)A_{\sigma_{\mathrm{Y}}}^2 C_6, \tag{71}$$

and

$$C_1 = \frac{(1+n)^2}{(1+2n)(2+3n)}, \qquad C_2 = \frac{n^2(3+5n)(1+n)}{(1+2n)^2(2+3n)^2}, \tag{72}$$

$$C_3 = \frac{2+3n}{2(1+n)(1+2n)}, \qquad C_4 = \left(\frac{n}{2+3n}\right)^3, \tag{73}$$

$$C_5 = \frac{n^2(3+4n)}{4(1+2n)^2(1+2n)^2}, \qquad C_6 = \frac{1}{(1+n)(2+n)}. \tag{74}$$

We see that the Hessian is well-defined for the following condition:

$$\boxed{\eta > 0 \text{ and } PL \geq \sigma_{\mathrm{Y}}.} \tag{75}$$

4 COMPUTING THE INTEGRALS $I_1(a,b,k)$, $I_2(a,b,k)$ AND $I_3(a,b,k)$

4.1 Computing $I_1(a,b,k)$

For

$$I_1(a,b,k) = \int_a^b \left(\frac{y-l}{L-l}\right)^k dy, \tag{76}$$

we set

$$Y \coloneqq \frac{y-l}{L-l}. \tag{77}$$

Then

$$dy = (L-l)dY. \tag{78}$$

When y varies from a to b, Y varies from $\frac{a-l}{L-l}$ to $\frac{b-l}{L-l}$. With the above change of variable, we have

$$I_1(a,b,k) = (L-l)\int_{\frac{a-l}{L-l}}^{\frac{b-l}{L-l}} Y^k dY = (L-l)\left[\frac{1}{k+1}Y^{k+1}\right]_{\frac{a-l}{L-l}}^{\frac{b-l}{L-l}}$$
$$= \frac{L-l}{k+1}\left(\frac{b-l}{L-l}\right)^{k+1} - \frac{L-l}{k+1}\left(\frac{a-l}{L-l}\right)^{k+1}. \quad (79)$$

Especially, for $k > -1$, we have

$$I_1(l,L,k) = \frac{L-l}{k+1}. \quad (80)$$

4.2 Computing $I_2(a,b,k)$

For

$$I_2(a,b,k) = \int_a^b \left(\frac{y-l}{L-l}\right)^k \log\left(\frac{y-l}{L-l}\right) dy, \quad (81)$$

we use the same change of variable, and have

$$I_2(a,b,k) = (L-l)\int_{\frac{a-l}{L-l}}^{\frac{b-l}{L-l}} Y^k \log Y dY$$
$$= (L-l)\left[\frac{Y^{k+1}\left((k+1)\log Y - 1\right)}{(k+1)^2}\right]_{\frac{a-l}{L-l}}^{\frac{b-l}{L-l}}$$
$$= \frac{L-l}{k+1}\left(\frac{b-l}{L-l}\right)^{k+1}\log\left(\frac{b-l}{L-l}\right) - \frac{L-l}{(k+1)^2}\left(\frac{b-l}{L-l}\right)^{k+1}$$
$$- \frac{L-l}{k+1}\left(\frac{a-l}{L-l}\right)^{k+1}\log\left(\frac{a-l}{L-l}\right) + \frac{L-l}{(k+1)^2}\left(\frac{a-l}{L-l}\right)^{k+1}. \quad (82)$$

Especially, for $k > -1$, we have

$$I_2(l,L,k) = -\frac{L-l}{(k+1)^2}. \quad (83)$$

4.3 Computing $I_3(a,b,k)$

For

$$I_3(a,b,k) = \int_a^b \left(\frac{y-l}{L-l}\right)^k \left(\log\left(\frac{y-l}{L-l}\right)\right)^2 dy, \quad (84)$$

again, we use the same change of variable, and have

$$I_3(a,b,k) = (L-l)\int_{\frac{a-l}{L-l}}^{\frac{b-l}{L-l}} Y^k (\log Y)^2 dY$$
$$= (L-l)\left[\frac{Y^{k+1}\left((k+1)^2(\log Y)^2 - 2(k+1)\log Y + 2\right)}{(k+1)^3}\right]_{\frac{a-l}{L-l}}^{\frac{b-l}{L-l}}$$
$$= \frac{L-l}{k+1}\left(\frac{b-l}{L-l}\right)^{k+1}\left(\log\left(\frac{b-l}{L-l}\right)\right)^2 - \frac{2(L-l)}{(k+1)^2}\left(\frac{b-l}{L-l}\right)^{k+1}\log\left(\frac{b-l}{L-l}\right)$$
$$- \frac{L-l}{k+1}\left(\frac{a-l}{L-l}\right)^{k+1}\left(\log\left(\frac{a-l}{L-l}\right)\right)^2 + \frac{2(L-l)}{(k+1)^2}\left(\frac{a-l}{L-l}\right)^{k+1}\log\left(\frac{a-l}{L-l}\right)$$
$$+ \frac{2(L-l)}{(k+1)^3}\left(\frac{b-l}{L-l}\right)^{k+1} - \frac{2(L-l)}{(k+1)^3}\left(\frac{a-l}{L-l}\right)^{k+1}. \quad (85)$$

Especially, for $k > -1$, we have

$$I_3(l,L,k) = -\frac{2(L-l)}{(k+1)^3}. \quad (86)$$

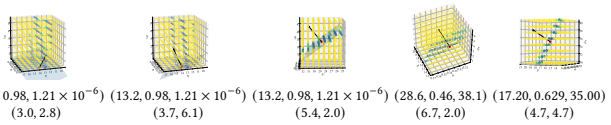

Fig. 1. We observed a few cases where the finite difference Hessians seemed inaccurate. We are showing the eigenvector corresponding to the largest eigenvalue and the plane normal to it (if the Hessian were accurate, this plane should align with the similarity set).

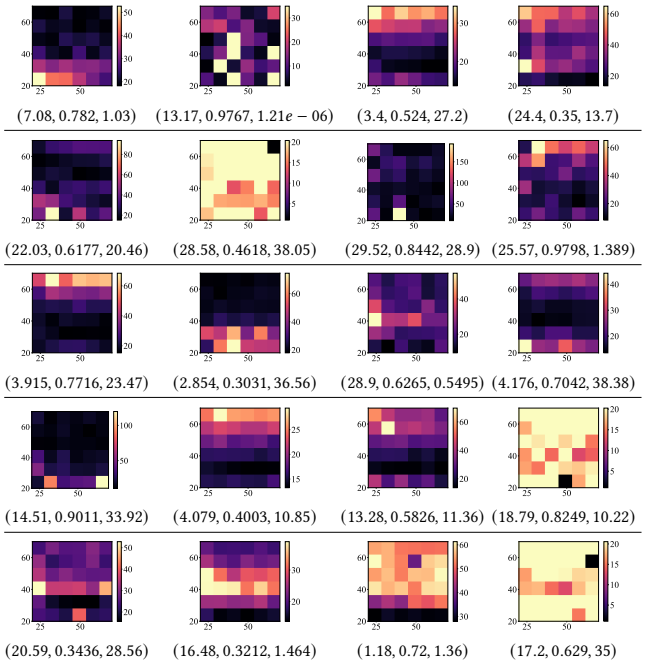

Fig. 2. For the 20 materials, we use finite differences to compute the Hessians of the loss. For visualization purposes, we show the condition numbers of the Hessians for different choices of the setup.

5 ON FINITE DIFFERENCE HESSIANS

We show a few cases where the Hessians computed using finite differences were inaccurate in Figure 1. Other cases (except for honey, $\mathbf{M} = (13.2, 0.98, 1.21 \times 10^{-6})$) seemed to be in a reasonable agreement. In Figure 2, we show the condition numbers computed using the Hessians from the finite differences. Although the condition numbers seem noisy, we can draw an insight that the setups with lower condition numbers can appear everywhere (for different materials), hence we decided to choose the first setup uniformly randomly. Of course, if we have prior knowledge of the material, we could further limit the choices of the first setup, but our assumption is that the user is not an expert and does not have much knowledge on the relation between the material parameters and the material behaviors.

6 DETAILED MPM AND MATCHED LOSS LANDSCAPES

We model the conversion function from $\mathbf{M} = (\eta, n, \sigma_Y)$ and $\mathbf{S} = (w, h)$ to PL using a polynomial of η, n, σ_Y, w, h, η^{-1}, n^{-1}, ${\sigma_Y}^{-1}$, w^{-1}, and h^{-1} up to second order as:

$$
\begin{aligned}
PL = \Theta_{PL}(\eta, n, \sigma_Y, w, h; \boldsymbol{c}) &= c_\eta \eta + c_n n + c_{\sigma_Y}(\sigma_Y + \varepsilon) + c_h h + c_w w \\
&+ c_{\eta^{-1}} \eta^{-1} + c_{n^{-1}} n^{-1} + c_{{\sigma_Y}^{-1}} (\sigma_Y + \varepsilon)^{-1} + c_{h^{-1}} h^{-1} + c_{w^{-1}} w^{-1} \\
&+ c_{\eta^2} \eta^2 + c_{\eta n} \eta n + c_{n^2} n^2 + c_{\eta \sigma_Y} \eta (\sigma_Y + \varepsilon) + c_{\eta h} \eta h + c_{n \sigma_Y} n (\sigma_Y + \varepsilon) \\
&+ c_{nh} nh + c_{\eta w} \eta w + c_{{\sigma_Y}^2} (\sigma_Y + \varepsilon)^2 + c_{nw} nw + c_{\eta n^{-1}} \eta n^{-1} \\
&+ c_{\sigma_Y h} (\sigma_Y + \varepsilon) h + c_{\eta \sigma_Y^{-1}} \eta (\sigma_Y + \varepsilon)^{-1} + c_{n \eta^{-1}} n \eta^{-1} + c_{\eta h^{-1}} \eta h^{-1} \\
&+ c_{h^2} h^2 + c_{\sigma_Y w} (\sigma_Y + \varepsilon) w + c_{n \sigma_Y^{-1}} n (\sigma_Y + \varepsilon)^{-1} + c_{\eta w^{-1}} \eta w^{-1} \\
&+ c_{\sigma_Y \eta^{-1}} (\sigma_Y + \varepsilon) \eta^{-1} + c_{n h^{-1}} n h^{-1} + c_{hw} hw + c_{\sigma_Y n^{-1}} (\sigma_Y + \varepsilon) n^{-1} \\
&+ c_{n w^{-1}} n w^{-1} + c_{h \eta^{-1}} h \eta^{-1} + c_{\sigma_Y h^{-1}} (\sigma_Y + \varepsilon) h^{-1} + c_{h n^{-1}} h n^{-1} + c_{w^2} w^2 \\
&+ c_{h \sigma_Y^{-1}} h (\sigma_Y + \varepsilon)^{-1} + c_{w \eta^{-1}} w \eta^{-1} + c_{\sigma_Y w^{-1}} (\sigma_Y + \varepsilon) w^{-1} + c_{\eta^{-2}} \eta^{-2} \\
&+ c_{w n^{-1}} w n^{-1} + c_{h w^{-1}} h w^{-1} + c_{w \sigma_Y^{-1}} w (\sigma_Y + \varepsilon)^{-1} + c_{\eta^{-1} n^{-1}} \eta^{-1} n^{-1} \\
&+ c_{\eta^{-1} \sigma_Y^{-1}} \eta^{-1} (\sigma_Y + \varepsilon)^{-1} + c_{w h^{-1}} w h^{-1} + c_{n^{-2}} n^{-2} + c_{\eta^{-1} h^{-1}} \eta^{-1} h^{-1} \\
&+ c_{n^{-1} \sigma_Y^{-1}} n^{-1} (\sigma_Y + \varepsilon)^{-1} + c_{{\sigma_Y}^{-2}} (\sigma_Y + \varepsilon)^{-2} + c_{\eta^{-1} w^{-1}} \eta^{-1} w^{-1} \\
&+ c_{n^{-1} h^{-1}} n^{-1} h^{-1} + c_{\sigma_Y^{-1} h^{-1}} (\sigma_Y + \varepsilon)^{-1} h^{-1} + c_{n^{-1} w^{-1}} n^{-1} w^{-1} \\
&+ c_{h^{-2}} h^{-2} + c_{\sigma_Y^{-1} w^{-1}} (\sigma_Y + \varepsilon)^{-1} w^{-1} + c_{h^{-1} w^{-1}} h^{-1} w^{-1} + c_{w^{-2}} w^{-2} \\
&+ c_1 \qquad (87)
\end{aligned}
$$

where $\varepsilon = 0.0001$ and $\boldsymbol{c} = \{c_\eta, c_n, \ldots\}$ are coefficients to be determined. We are using $(\sigma_Y + \varepsilon)$ instead of σ_Y as $\sigma_Y = 0$ is possible.

For training, we use 850 auxiliary landscapes in addition to the 200 landscapes $\mathfrak{L}$. We show the 20 materials used to generate $\mathfrak{L}$ in Figure 3, and the 445 materials used to generate the 850 auxiliary landscapes in Figure 4. The auxiliary landscapes were added to improve the conversion for materials near boundary of the material space $\mathfrak{M}$, hence the 445 materials were placed near the boundary.

For each of the training landscape L_i, we first compute the value $(PL)_i$ that would minimize the matching score described in the main paper for the corresponding material $\mathbf{M}_i$ and the setup $\mathbf{S}_i$. Then, we optimize the parameters $\boldsymbol{c}$ via:

$$
\boldsymbol{c} = \underset{\tilde{\boldsymbol{c}}}{\operatorname{argmin}} \sum_{i=1}^{1050} ((PL)_i - \Theta_{PL}(\mathbf{M}_i, \mathbf{S}_i; \tilde{\boldsymbol{c}}))^2, \qquad (88)
$$

using the 1,050 landscapes. We show the resulting coefficients in Table 3. Note that because the scaling of $\mathbf{H}^{\mathrm{PP}}$ does not matter when computing the loss normal, we can simply set P to an arbitrary value (2,500 in our code).

In Figures 5, 6, 7, 8, we show the 200 loss landscapes $\mathfrak{L}$ from MPM 3D simulations, as well as those from the plane Poiseuille flows with the setups computed using the conversion function (87). (Note that their scalings are adjusted for better visual comparison.)

We note that extrapolation is prone to an error. Although our 850 auxiliary landscapes are added to suppress the possibility of extrapolation, there are corner cases at (the very) vicinity of the boundary of the material space (especially for the lower end of the consistency parameter), where the estimated PL value can be smaller than σ_Y, in which case the Hessian of the plane Poiseuille flow does not exist. To mitigate the corner cases, one can introduce an offset to the PL values computed via the learned conversion map Θ_{PL}; during the setup finding, we can compute an offset δ common to all the candidate setups such that $PL + \delta \geq \sigma_Y$, and then return $PL + \delta + \varepsilon_0$ as the modified PL value, where $\varepsilon_0 = 10^{-6}$. In the optimizations for the real world materials and emulations shown in the paper, we did not encounter such corner cases, hence this modification was not invoked.

We may have post-publication updates on the conversion map. Please see our project page at http://www.cg.it.aoyama.ac.jp/yonghao/siga23/abstsiga23.html for any updates (and additional validations).

Table 3. Coefficients of Θ_{PL}.

c_η	4.0306617945	c_n	−543.33833895	c_{σ_Y}	−0.39644936694
c_h	2449.4279436	c_w	−1178.04427785	$c_{\eta^{-1}}$	−1.4997154788
$c_{n^{-1}}$	−162.942771915	$c_{{\sigma_Y}^{-1}}$	0.188073149715	$c_{h^{-1}}$	1.45292372775
$c_{w^{-1}}$	−1.2631178092500002	c_{η^2}	−0.12752455765499998	$c_{\eta n}$	−1.0874210193
c_{n^2}	519.1498323	$c_{\eta \sigma_Y}$	−0.012581743284	$c_{\eta h}$	35.388495647999996
$c_{n \sigma_Y}$	−0.38297933982	c_{nh}	1055.4582258	$c_{\eta w}$	−17.091957069000003
$c_{{\sigma_Y}^2}$	0.0203883526935	c_{nw}	−1249.0011963	$c_{\eta n^{-1}}$	−0.12292563689999998
$c_{\sigma_Y h}$	8.1838951821	$c_{\eta \sigma_Y^{-1}}$	$-5.1163500564000004e-05$	$c_{n \eta^{-1}}$	−0.013688615358
$c_{\eta h^{-1}}$	−0.01055746395	c_{h^2}	−43683.9639885	$c_{\sigma_Y w}$	−7.706071197
$c_{n \sigma_Y^{-1}}$	0.022644721242	$c_{\eta w^{-1}}$	−0.028196188317	$c_{\sigma_Y \eta^{-1}}$	$2.5654560426e-05$
$c_{n h^{-1}}$	0.52635351087	c_{hw}	21142.219527	$c_{\sigma_Y n^{-1}}$	0.42993512199
$c_{n w^{-1}}$	−1.9099255626	$c_{h \eta^{-1}}$	−0.059850779471999994	$c_{\sigma_Y h^{-1}}$	0.024744463524
$c_{h n^{-1}}$	9.071837864099999	c_{w^2}	12892.945824	$c_{h \sigma_Y^{-1}}$	0.06978780606599999
$c_{w \eta^{-1}}$	0.0072816866694	$c_{\sigma_Y w^{-1}}$	−0.013486781286	$c_{\eta^{-2}}$	0.000301032720945
$c_{w n^{-1}}$	−304.35359427000003	$c_{h w^{-1}}$	12.859676379	$c_{w \sigma_Y^{-1}}$	−0.0093745811115
$c_{\eta^{-1} n^{-1}}$	−0.0018862453962	$c_{\eta^{-1} \sigma_Y^{-1}}$	$-4.7967749181e-07$	$c_{w h^{-1}}$	27.66781116
$c_{n^{-2}}$	37.454037291	$c_{\eta^{-1} h^{-1}}$	$4.1407292223e-05$	$c_{n^{-1} \sigma_Y^{-1}}$	0.0067023002277
$c_{\sigma_Y^{-2}}$	$8.520888816e-07$	$c_{\eta^{-1} w^{-1}}$	$1.8194127633e-05$	$c_{n^{-1} h^{-1}}$	0.43541358003
$c_{\sigma_Y^{-1} h^{-1}}$	$6.6016072287e-05$	$c_{n^{-1} w^{-1}}$	−0.35355061368	$c_{h^{-2}}$	−0.051344184375
$c_{\sigma_Y^{-1} w^{-1}}$	$-1.578818934e-06$	$c_{h^{-1} w^{-1}}$	0.025526405322	$c_{w^{-2}}$	0.0293432249385
c_1	7666.914266599998				

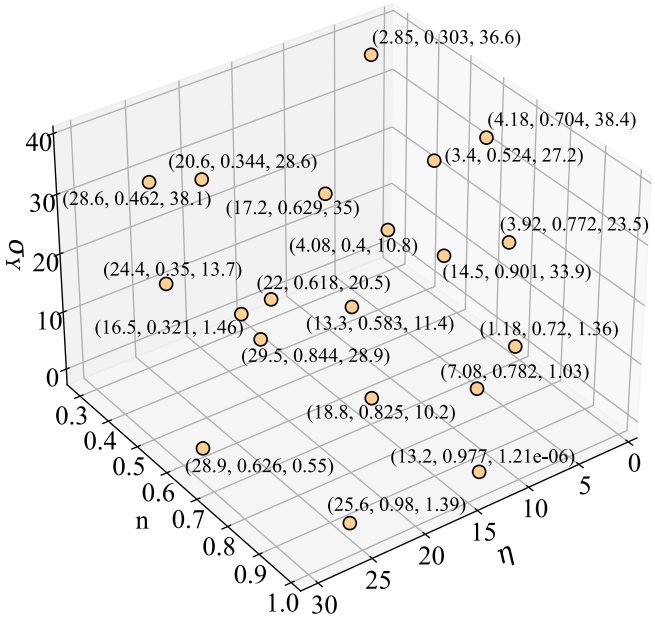

Fig. 3. We show the distribution of the material parameters of the 20 selected materials.

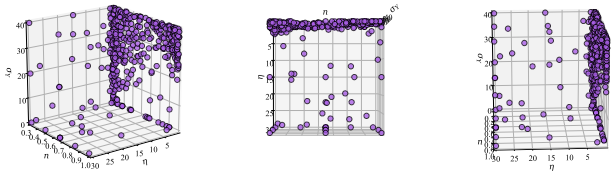

Fig. 4. We show the distribution of the material parameters of the 445 selected materials near the boundary of the material space $\mathfrak{M}$.

7 SILHOUETTE IMAGES

From the 200 material-setup pairs for $\mathfrak{L}$, we randomly choose 20 material-setup pairs and compare 1) loss landscapes of different views in Figure 9, and 2) silhouette images with low loss values at distant material parameters in Figures 10, 11, 12, 13, and 14. We see that different views resulted in almost identical loss structures and that distant material parameters can result in almost identical (low) loss values.

8 DETAILED EMULATION RESULTS

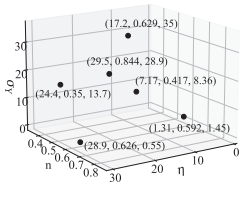

We show the chosen 6 materials in the right inset. We show the emulation results up to using four setups in Figures 15, 17, 18, 19, **??**, and 21. The black lines correspond to the single setup cases, and their results up to 700 simulation count are used as those for the first setups (orange lines) in the multiple setup cases; hence up to 700 simulation count, the black and orange lines are overlapping with each other. The black lines in the flow curve plots corresponds to the results at the last simulation counts of the single setup cases.

In Figure 16, we see that 1) using a second setup with the loss normal similar to the first setup and 2) using the frames from another view in place of the second setup both resulted in inferior results compared to using our method.

REFERENCES

Yun (Raymond) Fei, Christopher Batty, Eitan Grinspun, and Changxi Zheng. 2019. A multi-scale model for coupling strands with shear-dependent liquid. *ACM Trans. Graph.* 38, 6, Article 190 (2019), 20 pages. https://doi.org/10.1145/3355089.3356532

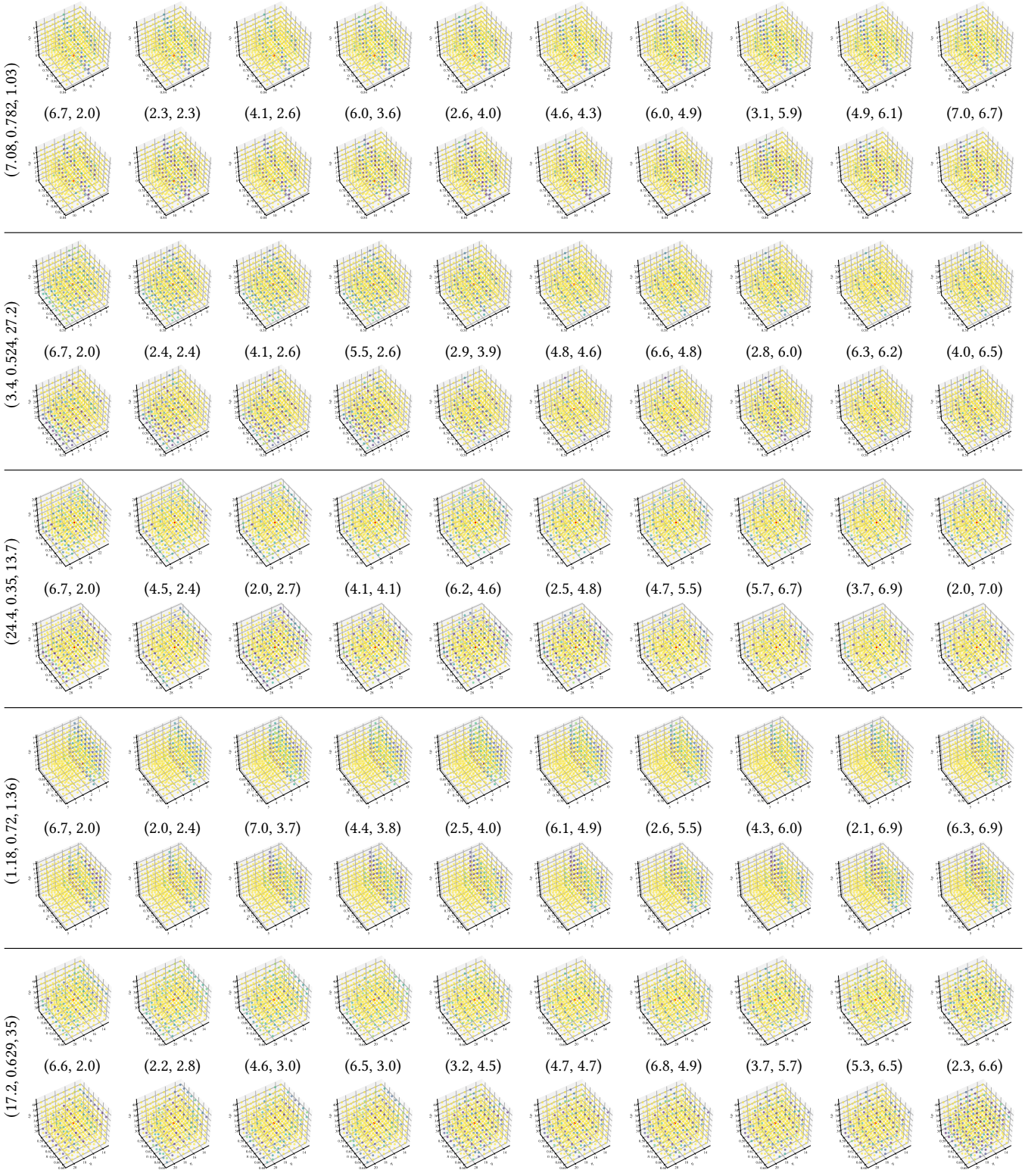

Fig. 5. For each material (whose material parameters are listed in the left and also shown as the red dots in the plots), we show the MPM 3D loss (top), the setups in (width, height) (middle), and the matched plane Poiseuille loss (bottom). Yellow dots indicate large loss values while purple (to blue) dots indicate low loss values.

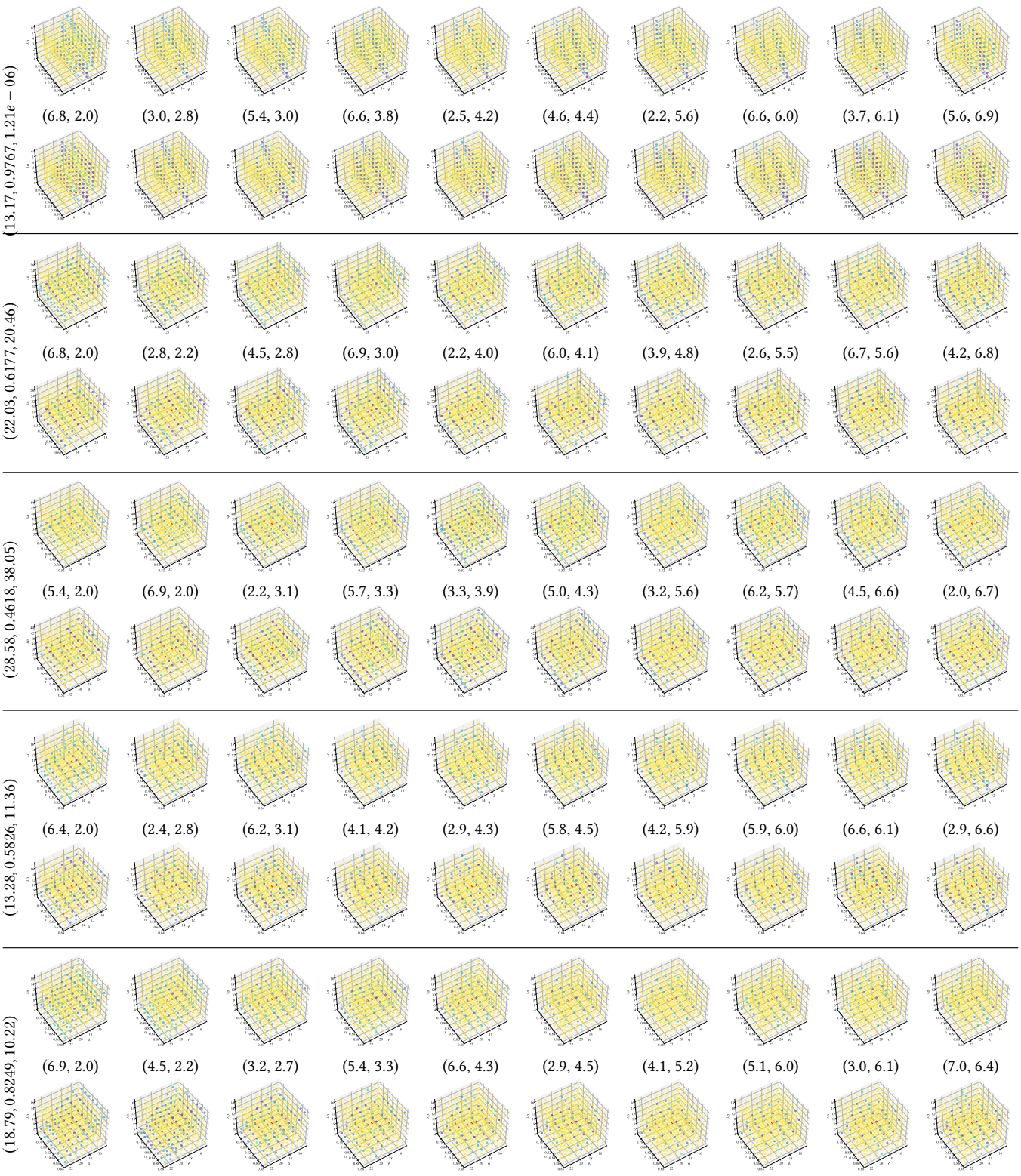

Fig. 6. For each material (whose material parameters are listed in the left and also shown as the red dots in the plots), we show the MPM 3D loss (top), the setups in (width, height) (middle), and the matched plane Poiseuille loss (bottom). Yellow dots indicate large loss values while purple (to blue) dots indicate low loss values.

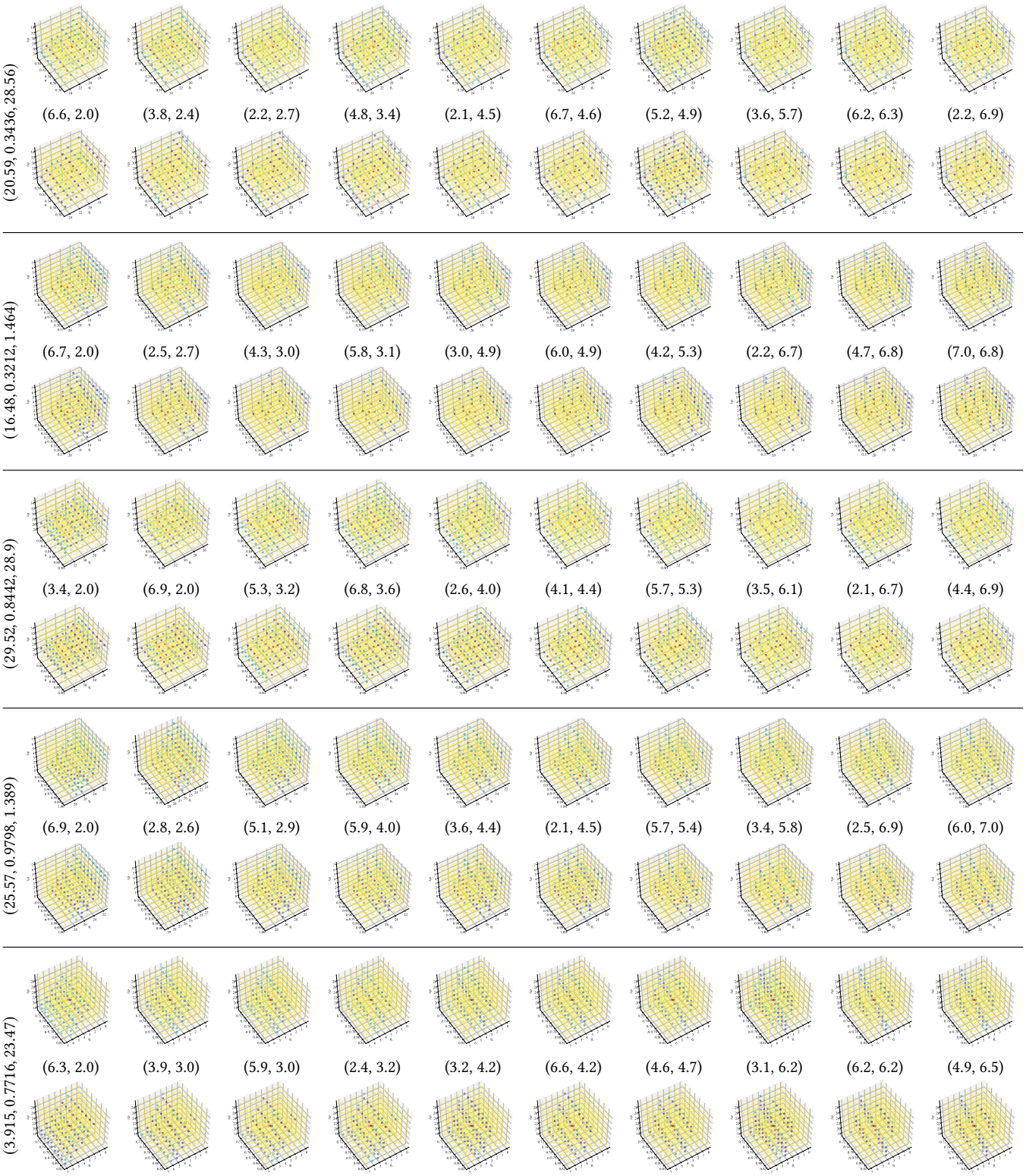

Fig. 7. For each material (whose material parameters are listed in the left and also shown as the red dots in the plots), we show the MPM 3D loss (top), the setups in (width, height) (middle), and the matched plane Poiseuille loss (bottom). Yellow dots indicate large loss values while purple (to blue) dots indicate low loss values.

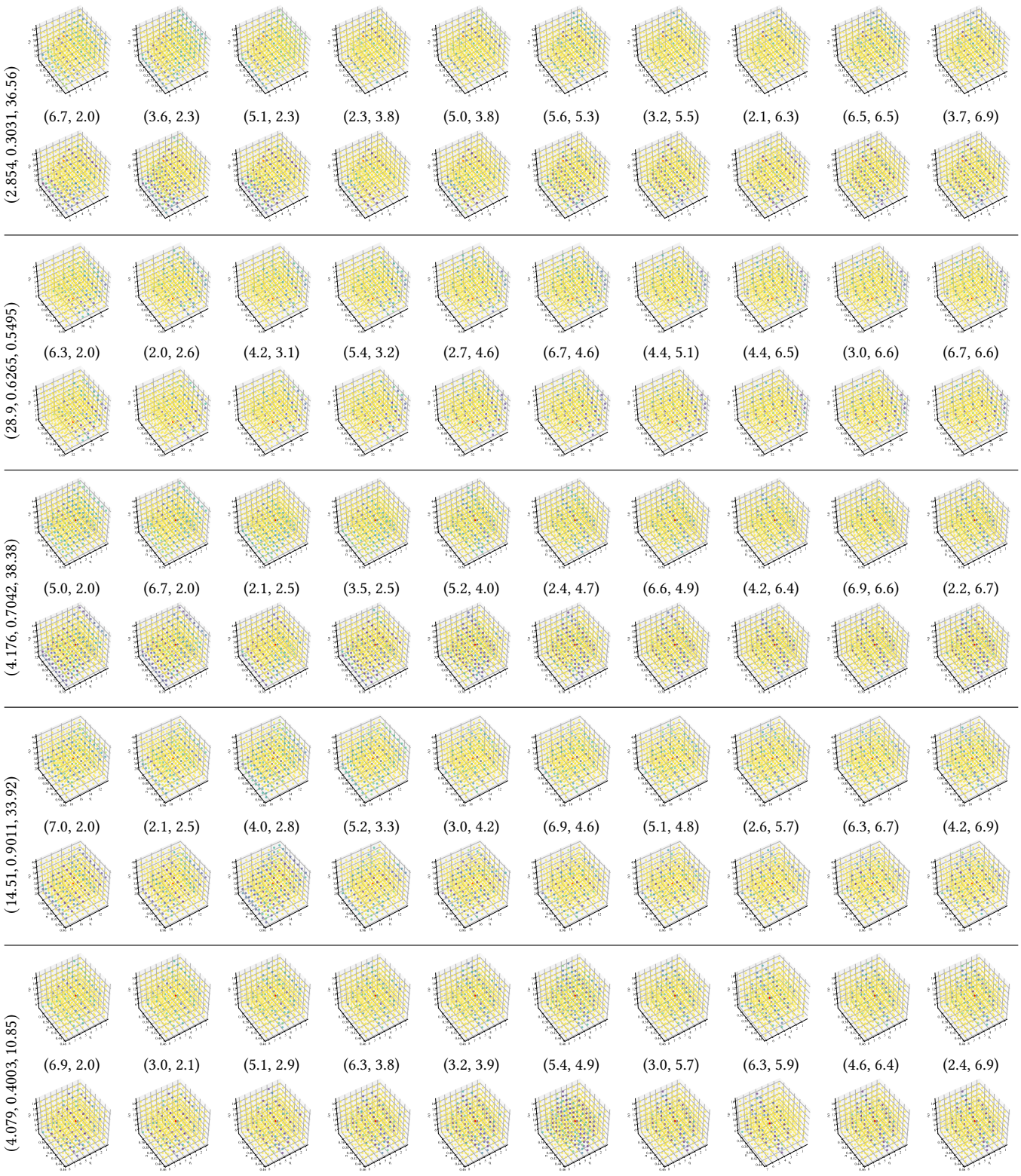

Fig. 8. For each material (whose material parameters are listed in the left and also shown as the red dots in the plots), we show the MPM 3D loss (top), the setups in (width, height) (middle), and the matched plane Poiseuille loss (bottom). Yellow dots indicate large loss values while purple (to blue) dots indicate low loss values.

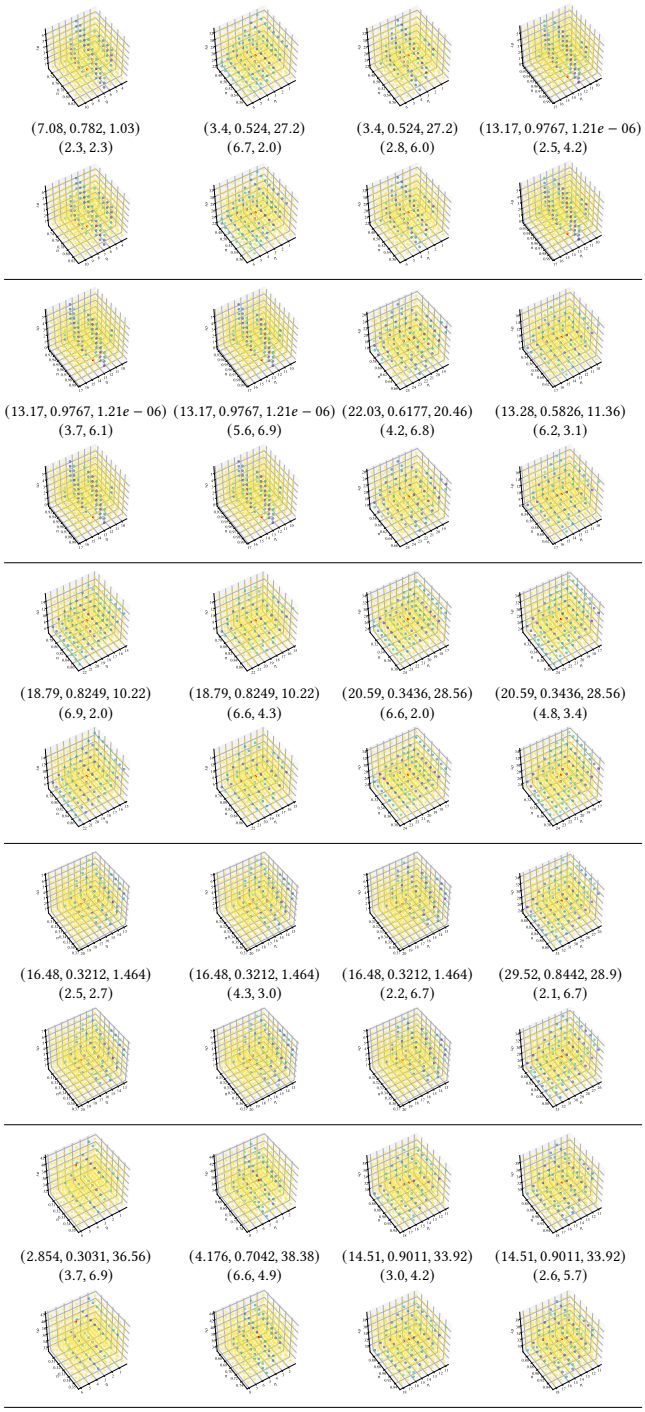

Fig. 9. For each row (separated by the horizontal lines), we compare the loss landscape of the original view (top) and that of a different view (bottom). In the middle, we list the material parameters (η, n, σ_Y) (also shown as the red dots in the plots) and the setup sizes (width, height).

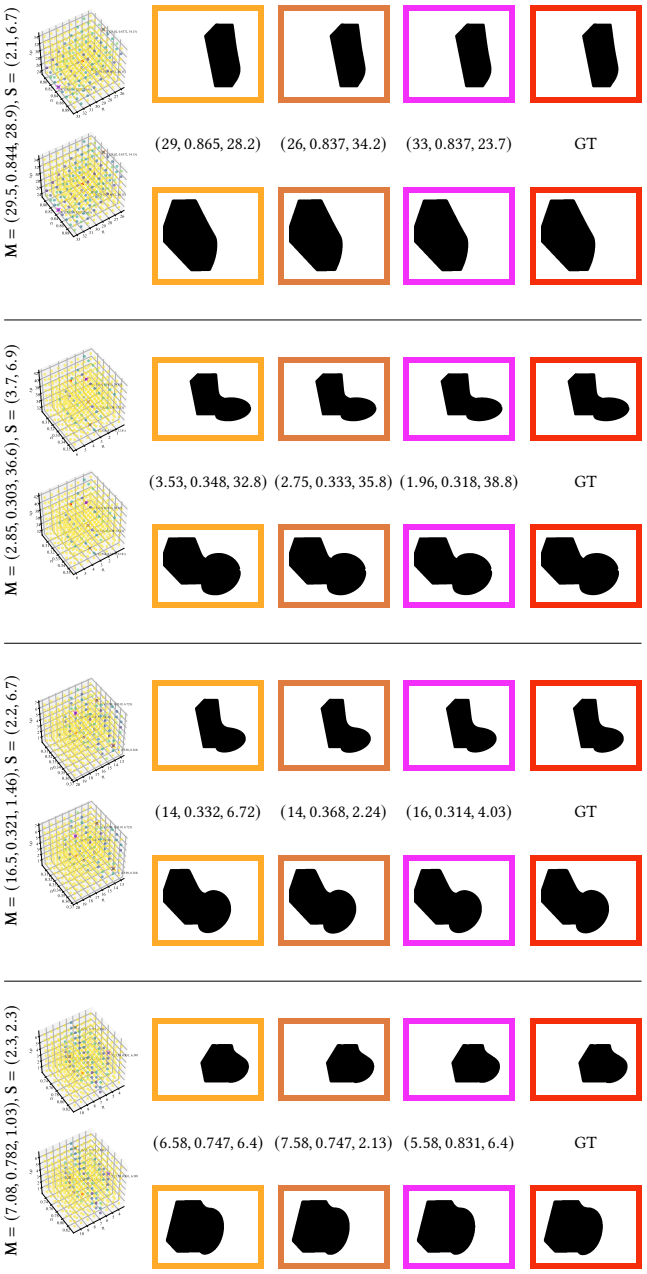

Fig. 10. For the material-setup pairs shown in the left, we show in the right their loss landscapes and silhouette images of the last frame, computed for two different views (corresponding to top and bottom rows).

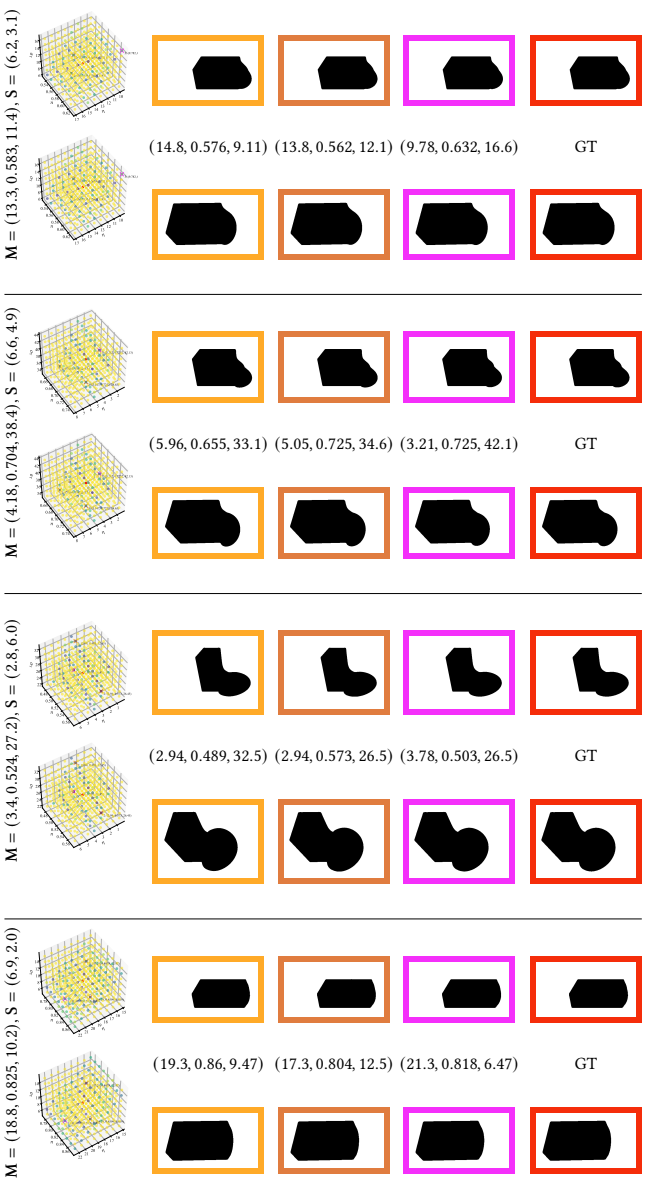

Fig. 11. For the material-setup pairs shown in the left, we show in the right their loss landscapes and silhouette images of the last frame, computed for two different views (corresponding to top and bottom rows).

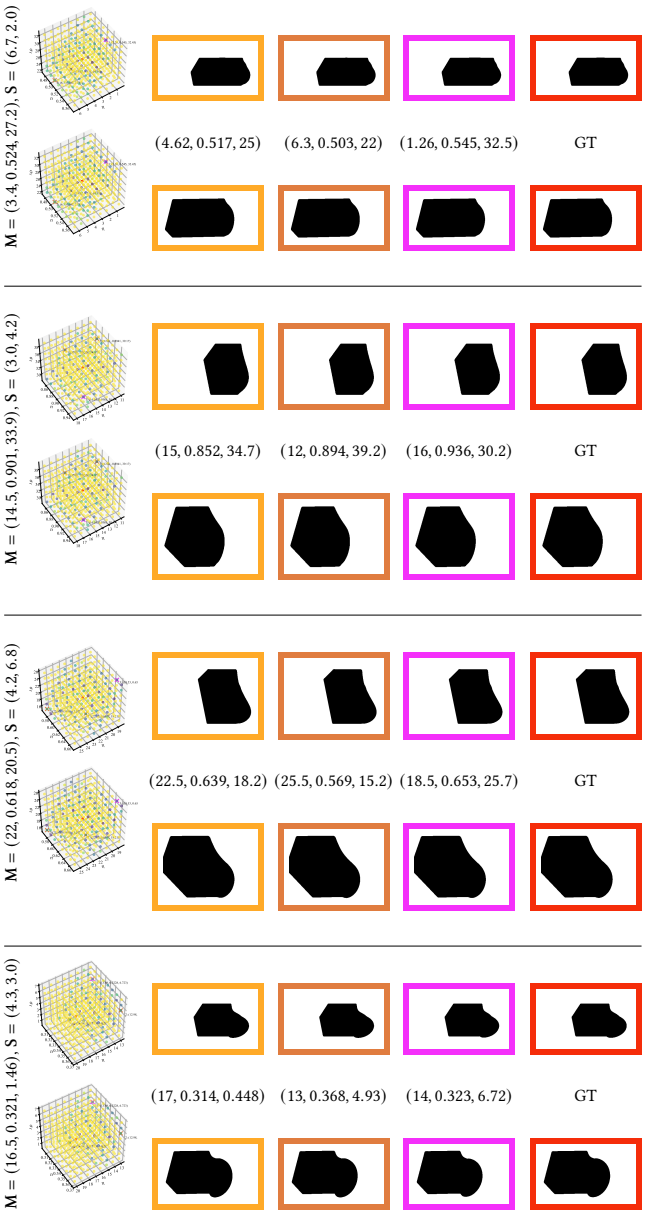

Fig. 12. For the material-setup pairs shown in the left, we show in the right their loss landscapes and silhouette images of the last frame, computed for two different views (corresponding to top and bottom rows).

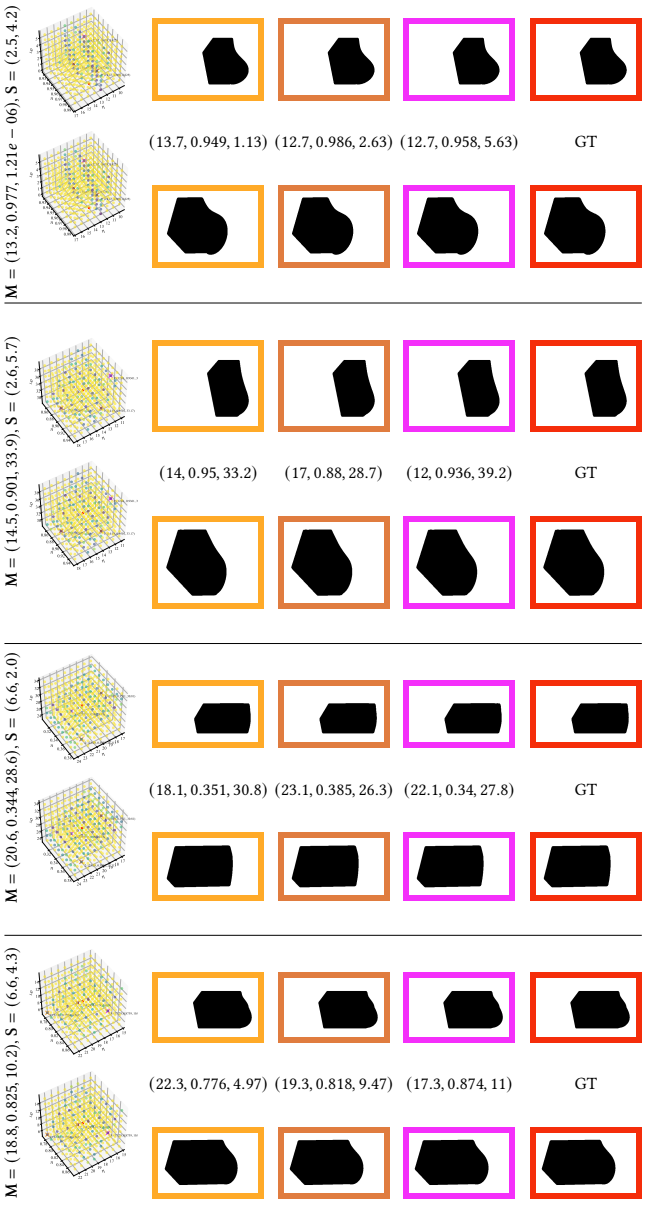

Fig. 13. For the material-setup pairs shown in the left, we show in the right their loss landscapes and silhouette images of the last frame, computed for two different views (corresponding to top and bottom rows).

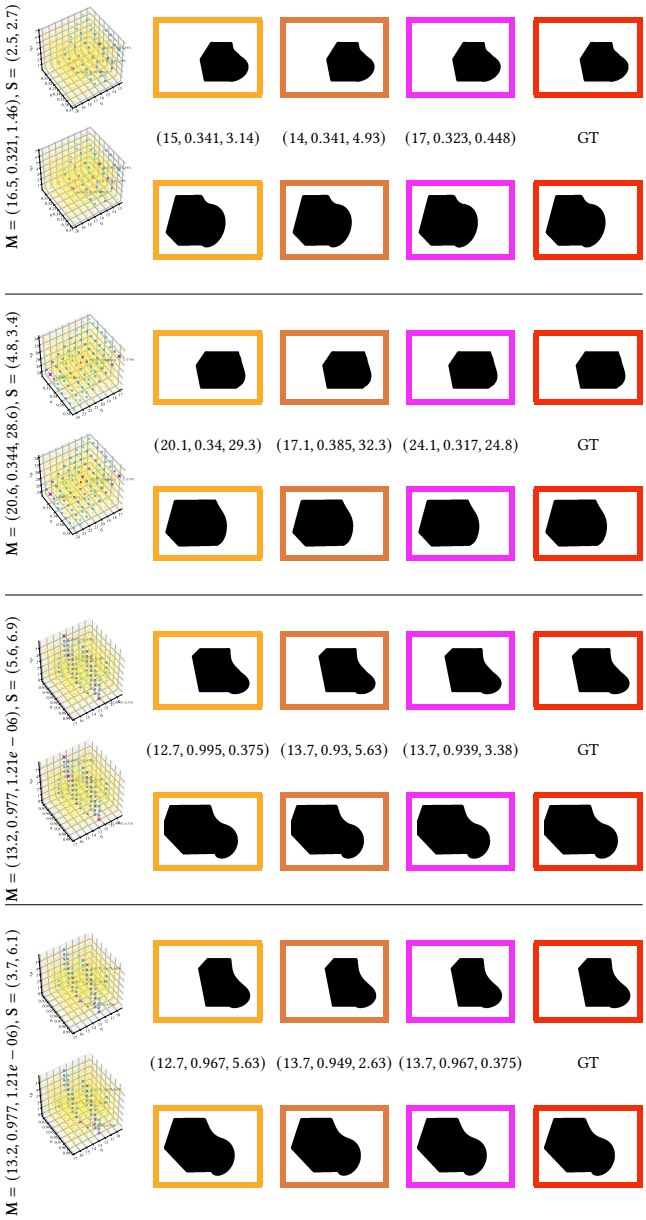

Fig. 14. For the material-setup pairs shown in the left, we show in the right their loss landscapes and silhouette images of the last frame, computed for two different views (corresponding to top and bottom rows).

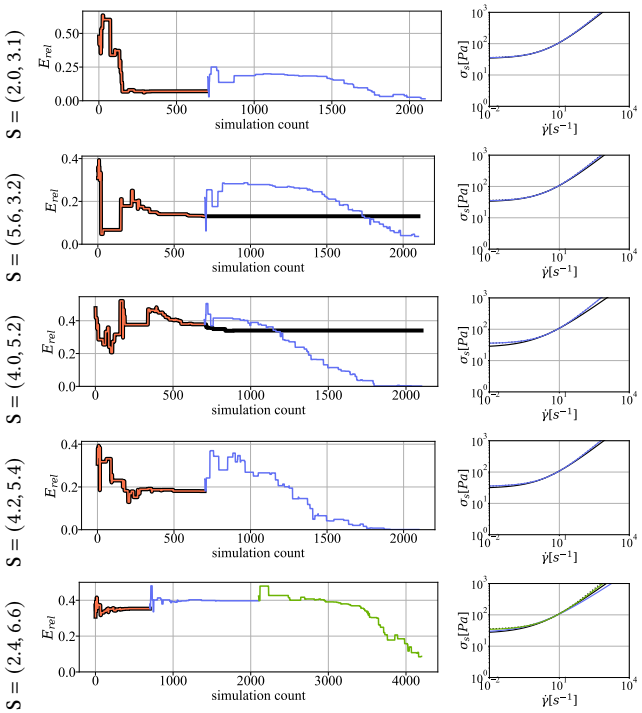

Fig. 15. Emulation results for $\mathbf{M} = (17.2, 0.63, 35.0)$. The chosen first setups are shown in the left. The middle plots show the relative error (vertical axis) as the simulation count (vertical axis) proceeds. As the relative error, we are plotting the error for the estimated material parameters having the lowest MPM 3D loss thus far. The decrease of the error is not monotonic because lower loss could mean larger relative error in the material parameters in some cases. Black lines correspond to the single setup case, and orange, blue, and green lines correspond to the first, second, and third setup in the multiple setup cases. In the right, we show the corresponding flow curves at the end of the estimation using the single setup (black), using two setups (blue), and using three setups (green).

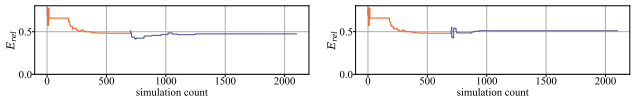

Fig. 16. For $\mathbf{M} = (28.9, 0.63, 0.55)$ and initial setup $\mathbf{S} = (5.1, 6.9)$, left: we select the second setup $\mathbf{S}_2 = (6.7, 6.6)$ such that its loss normal is similar to that of the first setup, yet the setup is distant from the first one; right: we use the frames from another view (for the first setup) in place of the second setup. We see that both resulted in inferior performance compared to the result in Figure 19 bottom.

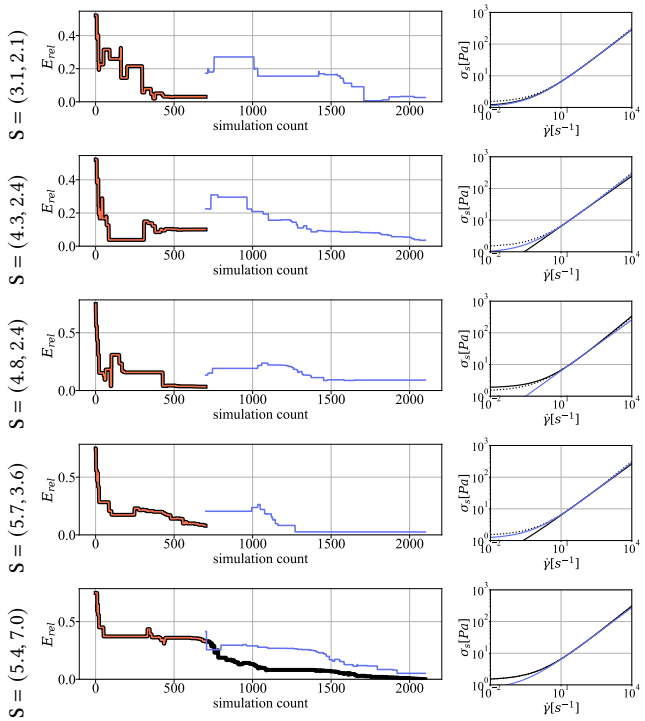

Fig. 17. Emulation results for $\mathbf{M} = (1.31, 0.59, 1.45)$. The chosen first setups are shown in the left. The middle plots show the relative error (vertical axis) as the simulation count (vertical axis) proceeds. As the relative error, we are plotting the error for the estimated material parameters having the lowest MPM 3D loss thus far. The decrease of the error is not monotonic because lower loss could mean larger relative error in the material parameters in some cases. Black lines correspond to the single setup case, and orange and blue lines correspond to the first and second setup in the multiple setup cases. In the right, we show the corresponding flow curves at the end of the estimation using the single setup (black), and using two setups (blue).

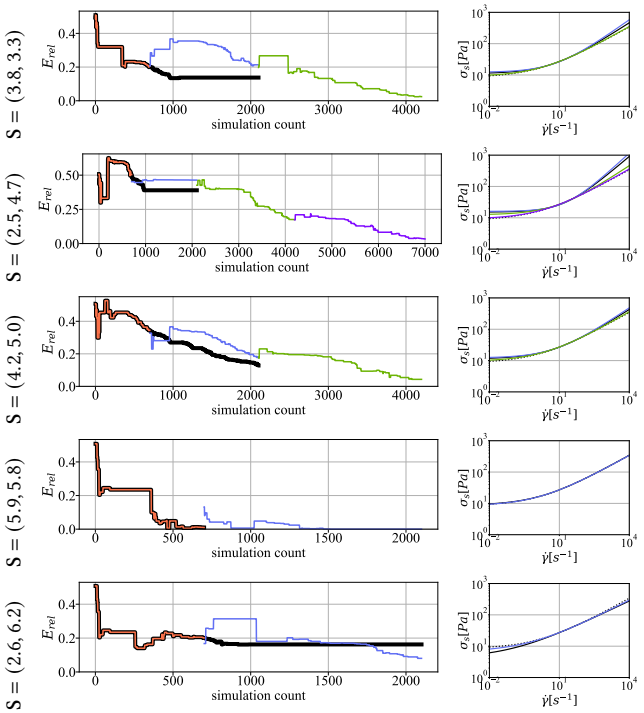

Fig. 18. Emulation results for $\mathbf{M} = (7.17, 0.42, 8.36)$. The chosen first setups are shown in the left. The middle plots show the relative error (vertical axis) as the simulation count (vertical axis) proceeds. As the relative error, we are plotting the error for the estimated material parameters having the lowest MPM 3D loss thus far. The decrease of the error is not monotonic because lower loss could mean larger relative error in the material parameters in some cases. Black lines correspond to the single setup case, and orange, blue, green, and purple lines correspond to the first, second, third, and fourth setup in the multiple setup cases. In the right, we show the corresponding flow curves at the end of the estimation using the single setup (black), using two setups (blue), using three setups (green), and using four setups (purple).

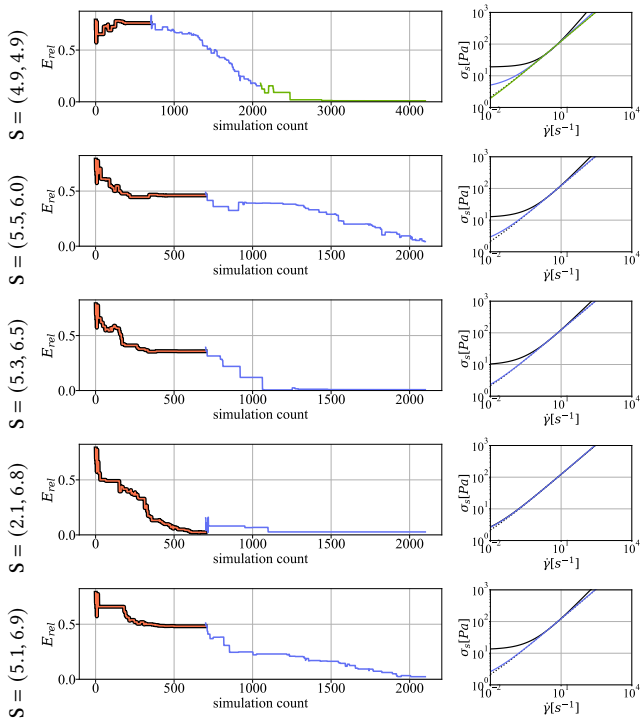

Fig. 19. Emulation results for $\mathbf{M} = (28.9, 0.63, 0.55)$. The chosen first setups are shown in the left. The middle plots show the relative error (vertical axis) as the simulation count (vertical axis) proceeds. As the relative error, we are plotting the error for the estimated material parameters having the lowest MPM 3D loss thus far. The decrease of the error is not monotonic because lower loss could mean larger relative error in the material parameters in some cases. Black lines correspond to the single setup case, and orange, blue, and green lines correspond to the first, second, and third setup in the multiple setup cases. In the right, we show the corresponding flow curves at the end of the estimation using the single setup (black), using two setups (blue), and using three setups (green).

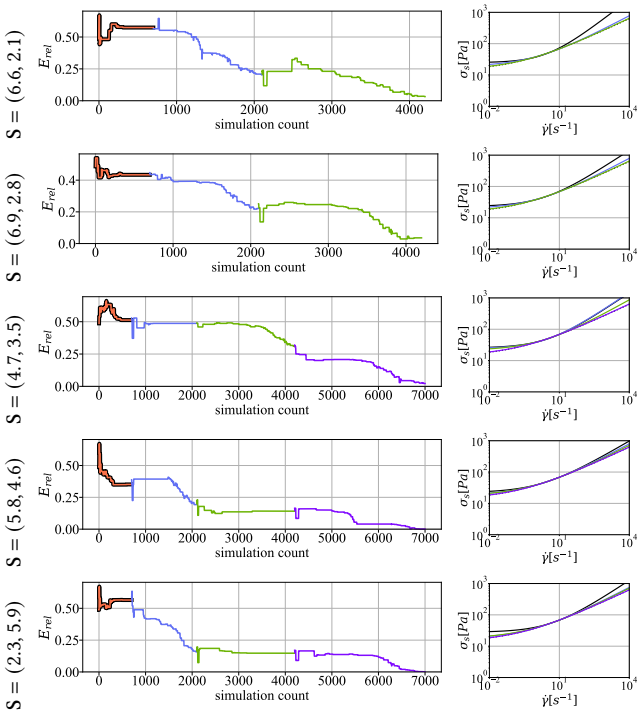

Fig. 21. Emulation results for $\mathbf{M} = (24.4, 0.35, 13.7)$. The chosen first setups are shown in the left. The middle plots show the relative error (vertical axis) as the simulation count (vertical axis) proceeds. As the relative error, we are plotting the error for the estimated material parameters having the lowest MPM 3D loss thus far. The decrease of the error is not monotonic because lower loss could mean larger relative error in the material parameters in some cases. Black lines correspond to the single setup case, and orange, blue, green, and purple lines correspond to the first, second, third, and fourth setup in the multiple setup cases. In the right, we show the corresponding flow curves at the end of the estimation using the single setup (black), using two setups (blue), using three setups (green), and using four setups (purple).